

Low-*P* melting of metapelitic rocks and the role of H₂O: Insights from phase equilibria modelling

Alfonso M. Sola¹ | Pavlina Hasalová² | Roberto F. Weinberg³ | Néstor O. Suzaño¹ | Raúl A. Becchio¹ | Fernando D. Hongn⁴ | Nilson Botelho⁵

¹CONICET-INENCO, Universidad Nacional de Salta, Salta, Argentina

²Centre for Lithospheric Research, Czech Geological Survey, Prague 1, Czech Republic

³School of Earth, Atmosphere and Environment, Monash University, Clayton, Victoria, Australia

⁴CONICET-IBIGEO, Universidad Nacional de Salta, Salta, Argentina

⁵Laboratório de Microsonda Eletrônica, Universidade de Brasília, Brasília, Brazil

Correspondence

Alfonso M. Sola, CONICET-INENCO-Universidad Nacional de Salta, Argentina. Email: sola.alfonso@gmail.com

Funding information

Agencia Nacional de Promoción Científica y Tecnológica - Fondo para la Investigación Científica y Tecnológica (ANPCyT - FONCYT), Grant/Award Number: PICT 2014-3507; Universidad Nacional de Salta

Handling editor: Michael Brown

Abstract

Water-fluxed melting has long been thought to have a minor influence on the thermal and chemical structure of the crust. We report here on amphibolite facies metasedimentary rocks from the 490–450 Ma Famatinian Orogen, in northwest Argentina, that have undergone water-fluxed incongruent biotite melting at relatively low temperature, which have produced and lost a significant volume of melt. The protoliths consist of the turbiditic Puncoviscana Formation (Neoproterozoic to Early Cambrian). The field area exhibits a condensed metamorphic field gradient, from greenschist to amphibolite facies suprasolidus conditions, recording a low pressure almost isobaric path, reaching peak conditions estimated at 700°C at 4 kbar. Thermodynamic modelling in the MnNCKFMASHTO system is applied to investigate melting at such low pressure as a function of water content. Calculations using a typical turbidite composition show how small amounts of added free H₂O may increase significantly the melt fraction with little or no change in either the melt or residual phase compositions. They indicate negligible difference in normative An–Ab–Or proportions and ferromagnesian contents between melts derived by dehydration and water-fluxed melts. The same is true for the content of H₂O dissolved in melts, which remains constant and the melt produced is granitic whether or not aqueous fluids are present. Thus, neither the residue nor the melt composition are indicators of the presence of aqueous fluids during anatexis. Recognizing the impact of small additions of H₂O to an anatectic terrane may therefore be difficult. The most significant change related to water-fluxing is the relative proportions of minerals and melt fraction, rather than the actual mineral assemblage. The modal proportion of feldspar decreased while those of cordierite and biotite increased in the residual assemblages, as <5 mol.% of free H₂O was added. The impact of this addition is to more than double the proportion of water-undersaturated melt to 25–30 mol.%. We have also developed a simple way to estimate how much melt a residual rock has lost, if the compositional trends of the protoliths are known. In summary, we find that even though the addition of small amounts of free H₂O impacts significantly on rock fertility, there is little obvious record in the field. The combined application of careful

Abbreviations: q, quartz; ksp, K-feldspar; pl, plagioclase; chl, chlorite; bi, biotite; mu, muscovite; g, garnet; cd, cordierite; opx, orthopyroxene; mt, magnetite; ilm, ilmenite; liq, silicate melt; ep, epidote; and, andalusite; sill, sillimanite; ky, kyanite.

petrological investigation and thermodynamic modelling is the key to identify the influence of aqueous fluids, and exploit systems that became open not only to fluid influx but also to the extraction of melt.

KEYWORDS

Famatinian Orogen, migmatite, NW Argentina, THERMOCALC, water-fluxed melting

1 | INTRODUCTION

The partial melting of metamorphic rocks within the continental crust is a process of major geological importance with orogenic-scale implications, since the presence of melt on grain boundaries weakens rocks, promoting faster deformation, ultimately influencing the way mountain belts evolve (Jamieson, Unsworth, Harris, Rosenberg, & Schulmann, 2011; Rosenberg & Handy, 2005; Vanderhaeghe, 2009; Vanderhaeghe & Teyssier, 2001). Moreover, extraction of melt from the lower continental crust, driven by buoyancy and tectonic forces, results in the chemical differentiation of the crust (Brown, 2013; Sawyer, 1994; Sawyer, Cesare, & Brown, 2011; Vielzeuf, Clemens, Pin, & Moinet, 1990). Crustal melting may involve the presence of a free H₂O phase, referred to as water-present or water-fluxed melting. Alternatively melting may involve the breakdown of a hydrous phase, such as biotite, muscovite or amphibole, and is referred to as dehydration melting, hydrate-breakdown melting or vapour- or fluid-absent melting. Dehydration melting reactions are incongruent and all the water is derived from the breakdown of hydrous minerals and melts produced are water-undersaturated. The production of mobile granitoid magmas is commonly considered to occur via incongruent dehydration melting (e.g. Brown, 1994; Clemens & Droop, 1998; Stevens & Clemens, 1993). However, there are a number of natural examples where water-fluxed melting appears to have played a significant role (Genier, Bussy, Epard, & Baumgartner, 2008; Jung, Hoernes, & Mezger, 2000; Sawyer, 2010; Ward, Stevens, & Kisters, 2008; Weinberg & Hasalová, 2015b). Water-fluxed melting can be either congruent, generally at low temperatures, or incongruent occurring at higher temperatures, where the melts are also water-undersaturated (Holtz & Johannes, 1991; Weinberg & Hasalová, 2015a). The latter may occur in the presence of low water activity fluids at P – T conditions above the water-saturated solidus, both below or above dehydration melting reactions. The presence of a water-rich fluid phase lowers the solidus temperature so that melting can take place at amphibolite facies conditions, with the potential to produce voluminous melt (e.g. Weinberg, Hasalová, Ward, & Fanning, 2013; Yardley & Barber, 1991).

Whilst water-saturated melts solidify upon decompression due to the negative slope of the P – T curve, many natural examples of water-fluxed melting have not generated water-saturated melts, as summarized by Weinberg and Hasalová (2015b). These melts formed in the presence of free water in what Clemens and Droop (1998) termed water deficient environments. Experimental studies on the anatexis of metapelites (Holtz & Johannes, 1991) determined that between 700 and 800°C melt remained water-undersaturated even though aqueous fluids were needed to trigger melting. Significantly, water-fluxed melts that are undersaturated are also upward mobile, with the potential to form plutonic intrusions and therefore impact the thermal and chemical structure of the crust (Weinberg & Hasalová, 2015a). Recognizing whether anatexis results from water-fluxed and dehydration-melting may not always be evident in the field, since both situations can generate peritectic minerals at P – T conditions anywhere between water-saturated solidus and dehydration melting curves (Brown, 2013; Jung et al., 2000, 2009; Kisters, Ward, Anthonissen, & Vietze, 2009; Otamendi & Patiño Douce, 2001; Ward et al., 2008; Weinberg & Hasalová, 2015b; Yardley & Barber, 1991).

The metamorphic sedimentary rocks of the Puncoviscana Formation exposed in Sierra de Molinos, part of the Famatinian Orogeny (490–450 Ma) in northwestern Argentina, provide a unique natural laboratory for the study of anatectic processes in low pressure, upper amphibolite facies conditions where voluminous melt was produced. These rocks exhibit a condensed metamorphic gradient, such that subsolidus and various suprasolidus and residual (melt-depleted) equivalents of the same lithology can be recognized in the field, making the area ideal to investigate the partial melting process. This study explores the P – T evolution of metapelites of the Puncoviscana Formation and the influence of water during anatexis, combining field-based, petrography and conventional geothermometry with a series of calculated isochemical phase diagrams (pseudosections). We investigate the impact of small additions of H₂O in melt reactions at low pressure, and then apply the results to investigate the nature of melting and the role of H₂O in the migmatites in Sierra de Molinos. The metamorphic evolution is interpreted with reference to

pseudosections in the MnNCKFMASHTO (MnO–Na₂O–CaO–K₂O–FeO–MgO–Al₂O₃–SiO₂–H₂O–TiO₂–O) system, integrating subsolidus and suprasolidus phase equilibria modelling.

2 | REGIONAL SETTING

In the Puna and Andean Eastern Cordillera of northwestern Argentina, many mountain ranges, displaying N–S elongation, are inliers where Neoproterozoic and Lower Paleozoic rocks crop out bounded by sedimentary deposits of Mesozoic and Cenozoic age. The N–S arrangement of such inliers is mainly due to the activity of Paleogene and Neogene Andean faults (Figure 1b), which reflect the overall E–W convergence between the Nazca and South America plates (e.g. Carrera, Muñoz, Sàbat, Mon, & Roca, 2006; Hongn et al., 2010, 2014 and references therein). This study deals with one of such inliers, the Sierra de Molinos, located at the southernmost part of the Eastern Cordillera, in the Calchaquí Valleys (Figure 1).

The sedimentary protolith of the metamorphic rocks consists of pelites and psammites comprising a turbiditic sequence assigned to the Puncoviscana Formation (Neoproterozoic to Early Cambrian; Aceñolaza, Miller, & Toselli, 1988; Jêzek, 1990). This was deposited in a large sedimentary basin at the west margin of Gondwana, extending over 800 km in the north-south direction from Bolivia (~22°S) to central Argentina (~27°S) and 150 km east-west roughly between 64 and 68°W (Ramos, 2008; Rapela, Toselli, Heaman, & Saavedra, 1990). U–Pb detrital zircon analysis from clastic sequences of this unit confirmed a maximum depositional age of late Early Cambrian based on the youngest detrital zircon population of *c.* 534–523 Ma (Adams, Miller, Toselli, & Griffin, 2008). Traditionally, it has been assumed that the Puncoviscana Formation was metamorphosed during at least two overlapping Palaeozoic orogenic episodes, the Pampean and the Famatinian events associated with magmatic arcs. In the Pampean event, the rocks were tightly folded and affected by low-grade metamorphism during the Early to Middle Cambrian (Aceñolaza, Miller, & Toselli, 2000). During the Famatinian Orogeny (*c.* 435–490 Ma), these rocks were metamorphosed into phyllites, schists, gneisses, culminating in anatectic migmatites and associated plutonism (Becchio, Lucassen, Kasemann, Franz, & Viramonte, 1999; Büttner et al., 2005; Insel et al., 2012; Lucassen et al., 2000; Rossi, Tosselli, & Durand, 1992; Sola, Becchio, & Pimentel, 2013). Therefore, the western margin of Gondwana could have been affected by successive events of medium to high-grade metamorphism during the Early Palaeozoic (Lucassen & Becchio, 2003). However, Pampean and Famatinian metamorphic and magma crystallization ages

seem to be continuous and occur in the same areas, especially in the northwestern Argentina and north of Chile (Lucassen & Becchio, 2003; Lucassen, Becchio, & Franz, 2011; Lucassen et al., 2000; Pankhurst, Rapela, & Fanning, 2000).

Deformation recorded is dominantly, marked by ductile shear zones developed during the Ordovician (Büttner et al., 2005; Finch, Weinberg, Fuentes, Hasalová, & Becchio, 2015; Hippertt & Hongn, 1998; Hongn, Mon, Cuevas, & Tubia, 1996). Emplacement of granite plutons derived from anatexis occurred largely between 480 and 460 Ma along with high-grade metamorphism and associated with N–S and NW–SE shear zones (Bahlburg, Berndt, & Gerdes, 2016; Büttner et al., 2005; Finch et al., 2015). However, the precise age relationships between magmatism, metamorphism and deformation are not well known (Hongn & Becchio, 1999; Hongn et al., 1996). Wegmann, Riller, Hongn, Glodny, and Oncken (2008), suggested that ductile deformation could have been active during magmatism and persisted afterwards under greenschist facies *P–T* conditions, reporting Rb–Sr mineral (white mica and K-feldspar) isochron ages of 437 ± 4 Ma and 428 ± 5 Ma for mylonitic rocks in a shear zone, located ~25 km south of the study area (Agua Rosada Shear Zone). Finch et al. (2015) also inferred a similar development for the Pichao Shear Zone, further south.

Migmatites a few kilometres north of the study area yielded a U–Pb monazite age of *c.* 467 Ma (Lork & Bahlburg, 1993), and of *c.* 470 Ma in the Sierras de Quilmes, overlapping with ages obtained for granitic plutonism (Büttner et al., 2005). Likewise, new U–Pb zircon dating by TIMS and SHRIMP methods in the Cachi mountain range yields similar ages for the migmatization (472 ± 11 Ma) and the emplacement of granites (479.7 ± 3.5 Ma; Hongn et al., 2014). In the study area, LA-ICPMS U–Pb zircon dating from granitoids and migmatites provided identical ages within the analytical errors, indicating that the metamorphic peak and granite generation occurred at *c.* 470 Ma (Sola et al., 2013).

2.1 | Metamorphism and field relationships in Sierra de Molinos

A preliminary description of metamorphism in Sierra de Molinos was provided by Sola et al. (2013). The Puncoviscana Formation rocks show a continuous transition from low-grade rocks to migmatites (metatexites and diatexites). The metamorphic grade increases from W to E, from greenschist facies phyllites and schists to upper amphibolite facies migmatites on the eastern side of the mountain range (Figure 1b). The mineral assemblages appear to be the result of a progressive increase in temperature without a significant change in pressure, with classic features of high

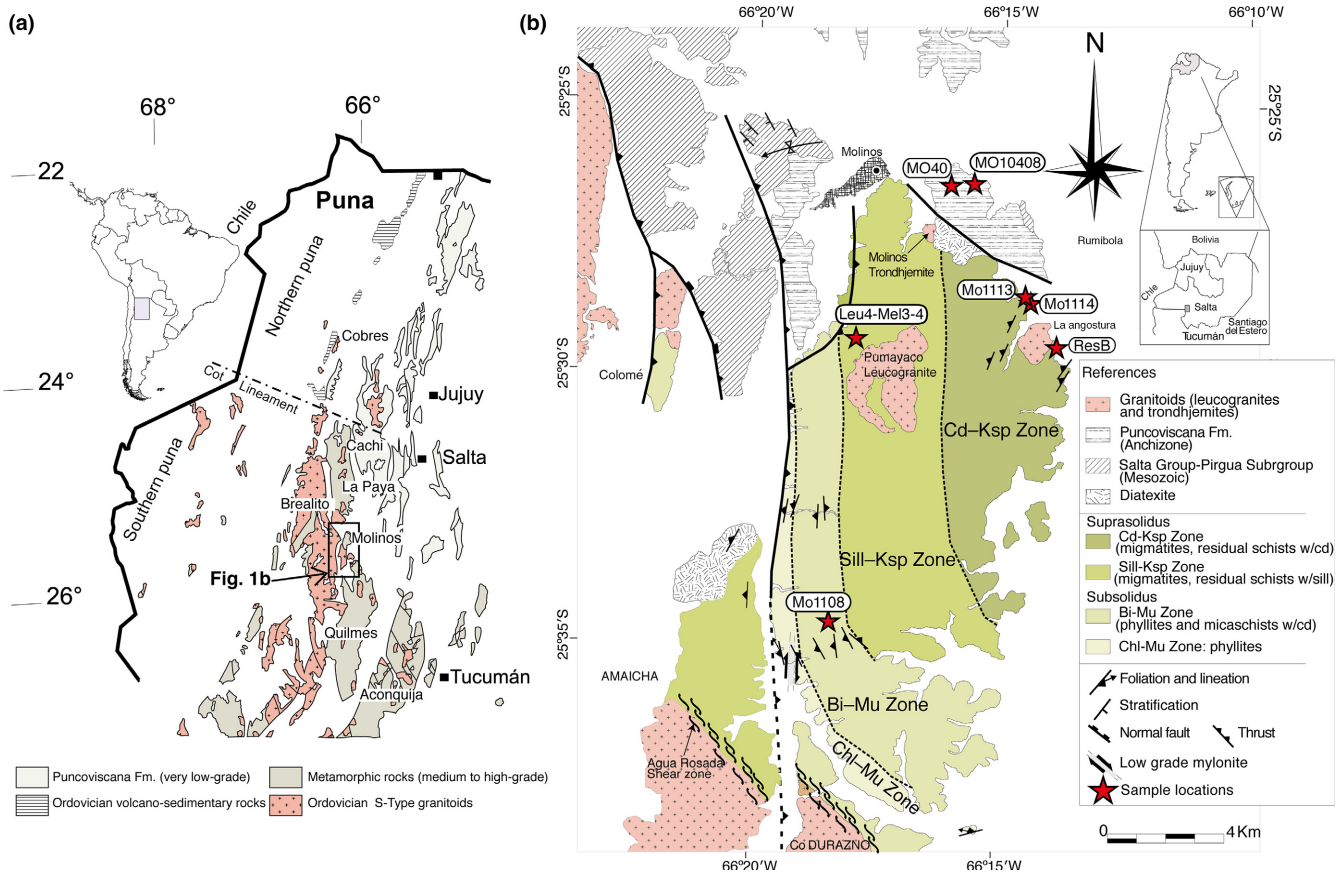


FIGURE 1 (a) Simplified geological map of NW Argentina showing the outcrops of pre-Devonian basement units: the very low-grade Puncoviscana Formation (Neoproterozoic to Cambrian), its metamorphic equivalents medium to high grade, and Ordovician granitoids. The main localities of Calchaquí Valleys are shown. (b) Distribution of metamorphic zones in Sierra de Molinos in order of increasing metamorphic grade: chl-mu; mu-bi; sill-ksp; cd-ksp

temperature and low- P conditions (e.g. Spear, Kohn, & Cheney, 1999): (1) no kyanite has been found in the area, but sillimanite is widespread as the metamorphic grade increases, (2) cordierite is common and occurs from low to intermediate metamorphic grade and also as a peritectic phase associated with leucosomes within the higher grade migmatites, (3) garnet is rare or absent in most metamorphic units, and (4) migmatites are developed above the so-called “second sillimanite isograd” with progression from sillimanite–K-feldspar assemblages to cordierite–K-feldspar assemblages in the highest grade migmatites. The migmatite zone contains variably deformed pegmatite and aplitic dykes (Figure 2a), small granitic bodies (metre to decametre in size) intruding migmatites. The temperature during partial melting was estimated by Sola et al. (2013) from the saturation temperature of zircon and monazite in residuum-poor leucosome and leucogranite samples, to be in the ranges 624–698°C and 620–687°C, respectively.

Four principal rock types have been recognized in the study area (Sola & Becchio, 2012; Sola et al., 2013): (1) non-migmatitic metasedimentary rocks: pelites, psammities and minor calc-silicates; (2) metatexite migmatites; (3)

diatexite migmatites, and (4) intrusive rocks, i.e. leucogranites, trondhjemites and pegmatite/aplitic dykes. Granite intrusions range in shape from thin granite streaks to wider dykes, sheets and plutons. Granitic rocks are typically peraluminous as indicated by the presence of sillimanite and/or cordierite in some of them, or more generally two micas. This together with their co-existence with migmatites suggests that they were derived from anatexis of metasedimentary rocks of the Puncoviscana Formation (Sola et al., 2013). However, the recognition of several intrusion episodes and the pervasive occurrence of pegmatites suggests that the major source of intrusive rocks is located somewhere deeper in the crust (Sola et al., 2013; Figure 2a).

Three main foliations are recognized in lower grade rocks. S_0 is the primary sedimentary bedding; S_1 is the axial planar foliation associated with isoclinal folds; and S_2 is a superimposed second axial planar cleavage, associated with refolding of the isoclinal folds. S_2 is the dominant tectonic foliation in the area. Only a rough cleavage can be recognized in psammitic layers, while a pervasive slate cleavage is present in pelitic layers.

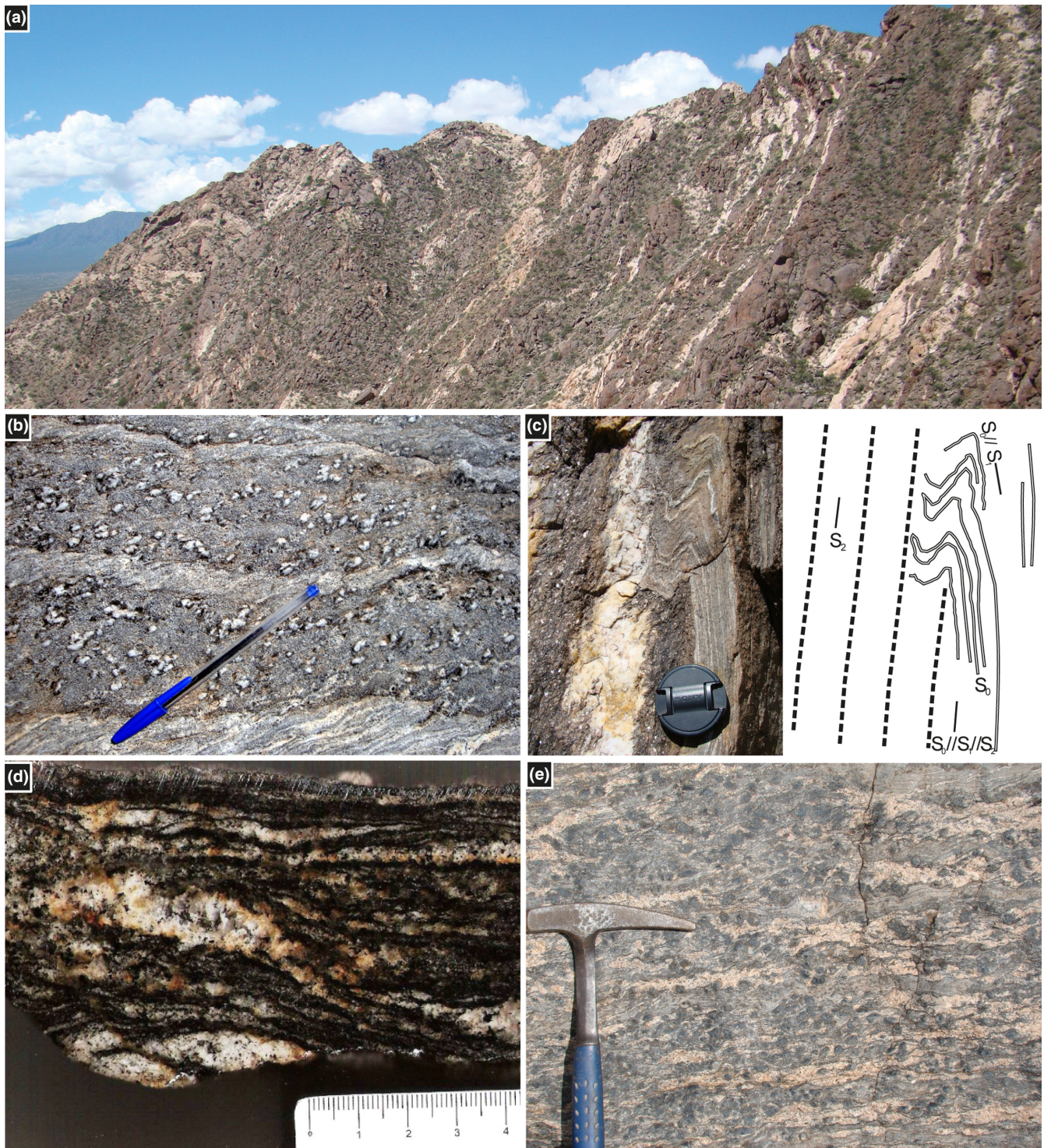


FIGURE 2 Photographs of structures: (a) Variably deformed pegmatites and aplitic dykes and small plutons hosted in the cd–ksp zone suggesting syn-tectonic or pre-tectonic emplacement. (b) Bedding preserved in migmatite from the sill–ksp zone, with abundant sillimanite (white aggregates) delineating a foliation in pelitic layers that is oblique to bedding parallel to the pen. (c) Spatial relationship between foliations in migmatite. Isoclinal fold preserved in psammitic layer showing the parallel orientation of S_0 , S_1 and S_2 in fold limbs. (d) Slice of stromatic metatexite from sill–ksp zone. (e) Stromatic metatexite from the cd–ksp zone showing numerous cordierite grains as darker grey rounded spots

The grain size increases with metamorphic grade from W to E. This is accompanied by a change in the type of foliation from a fine-grained slaty cleavage to migmatitic

banding, especially well-developed in stromatic metatexites. With increasing metamorphic grade, pegmatite and aplitic dykes are also more common and deformation becomes

more complex and heterogeneous. The spatial-temporal relationships between different foliations can be observed locally (Figure 2b). Figure 2c shows outcrops where the angular relations between different foliations in rocks that have experienced partial melting can be identified. Figure 2b shows fibrolitic sillimanite confined to metapelitic layers that are aligned with the metamorphic foliation (S2) and oblique to bedding (S0/S1). The same relationships can be found in higher grade migmatites where cordierite porphyroblasts from pelitic layers are aligned with S2 and oblique to S0/S1. Migmatitic rocks have stromatic banding, consisting of interlayered leucocratic and melanocratic bands, with lateral continuity (Figure 2d,e). Migmatites with net-structured leucosomes are common (Figure 3a,c). In these migmatites, the leucosomes represent felsic magma that was extracted from the matrix and accumulated in low-pressure sites such as shear bands or interboudins necks (Brown, 1994; Marchildon & Brown, 2003; McLellan, 1988; Sawyer, 1991, 1994). Many of these structures (e.g. Figure 3b) are good examples of pucker or collapse structures reflecting melt-loss from these sites (e.g. Bons, Druguet, Castaño, & Elburg, 2008). This is evidence that deformation was simultaneous with anatexis. Also, the lack of significant intracrystalline deformation of feldspar and quartz in most leucosomes, supports the inference that deformation occurred in the presence of melt.

Diatexites in Sierra de Molinos show a considerable range in morphologies and two main types can be recognized based on textural and mineralogical aspects: leucocratic diatexites and mesocratic diatexites. Leucocratic diatexites occur as metre-scale bodies showing intrusive relationships with the metatexites. Locally these bodies may connect with small granitic bodies and granitic dykes. Rafts of stromatic metatexites with internal layering may be present inside these leucocratic bodies (Figure 3d). Mesocratic diatexites display greater contents of mafic minerals implying less efficient residuum segregation. The contacts between these diatexites and the host metatexites are transitional suggesting local derivation. See Sola et al. (2013) for additional details.

3 | PETROGRAPHY

The petrographic features of rocks from each different zone are described below in order of increasing metamorphic grade.

3.1 | Anchizone

The lowermost grade Puncoviscana Formation rocks in the northeast part of Figure 1b, are composed predominantly of cm- to dm-scale layers of contrasting composition

inferred to be bedding. The layering consists of alternating chlorite-rich pelitic layers, and quartz-feldspar-rich psammitic layers with subordinate calc-silicate rocks (Figure 4a). Pelitic domains consist essentially of chlorite, white mica, quartz plus tourmaline, zircon, monazite and opaques as accessory minerals. Psammitic domains are composed of quartz, feldspar, minor chlorite and accessory rutile, monazite, zircon, tourmaline and opaque minerals. Some pelitic layers may contain dark (<2 mm diameter) poikiloblasts, which represent cordierite sometimes preserved showing sector twinning (Figure 4b), but more generally altered to fine-grained mica.

3.2 | Chlorite–muscovite zone

This zone consists of phyllites dominated by chlorite and muscovite that grade eastwards into cordierite-bearing phyllites and micaschist of the bi–mu zone. Compared to the anchizone where very fine-grained slates dominate, the rocks in this zone are slightly coarser-grained and phyllites are the principal rock type (Figure 4c). The assemblage is chlorite, muscovite, quartz and plagioclase, with subordinate biotite and accessory ilmenite, tourmaline, zircon and monazite. Recognition of minor amounts of biotite indicates that greenschist facies was reached. Small garnet porphyroblasts (<1 mm) can be found locally in some of these phyllites, and their growth could have been limited to specific bulk compositions (e.g. Mn-rich rocks), since its distribution does not allow tracing a mineral isograd or a garnet zone in the field. Internally these garnet porphyroblasts preserve folded inclusion trails suggesting synkinematic growth with S2 foliation.

3.3 | Muscovite–biotite zone (sample MO1108)

The muscovite–biotite zone is characterized by the absence of chlorite. This zone is dominated by cordierite-bearing micaschists (Figure 4d) comprising quartz, biotite, muscovite, cordierite, plagioclase±sillimanite±ilmenite±magnetite. Their common texture is porphyro-lepidoblastic, usually displaying quartz-rich (Q) and mica-rich (M) domains (Figure 4d). Towards the east, there is a gradual increase in grain size and modal proportion of biotite, induced by higher metamorphic conditions. In this zone cordierite is found as porphyroblasts (2–5 mm long) containing small inclusions of quartz and mica. The foliation is defined by preferred orientation of muscovite and biotite (Figure 4e) and is generally oblique to the porphyroblast elongation, and the matrix has undergone post-porphyroblast coarsening as indicated by the smaller grain size of inclusions compared to same minerals in the matrix. Towards the contact with the sill–ksp zone and the migmatite front, small amounts of sillimanite (fibrolite) are found



FIGURE 3 Anatectic structures: (a) Net structure defined by two sets of leucosomes, one parallel to foliation (only slightly lighter coloured than surrounding rock) and a second in short, dilatant structures oriented perpendicular to the dominant N–S foliation (cd–ksp zone). (b) Pucker structure in which layering collapse into apparent interboudin partitions reflecting melt-loss from these sites (migmatite form sill–ksp zone). (c) Leucosomes in low- P boudin necks in stromatic migmatites (cd–ksp zone). (d) Leucocratic diatexite with folded and partly disrupted biotite-rich residual rafts and schlieren

forming fibrous aggregates replacing cordierite (Figure 4f). The upper limit of this zone is marked by the complete disappearance of primary muscovite, the appearance of the first leucosomes and the presence of sillimanite (fibrolite), which along with the biotite, define the main foliation of higher-grade rocks.

An important feature of this zone is the presence of layers that are rich in magnetite (Figure 5). This is best seen in sample MO1108, which will also be used here to determine P – T condition of the mu–bi zone. This rock has relatively coarse matrix magnetite and cordierite porphyroblasts with numerous inclusions of rounded magnetite, in the same proportion as coarser magnetite in the matrix (compare Figure 5b,d). The cordierite porphyroblast rims are partially replaced by fine-grained mica but the centre is usually preserved (Figure 5a). Backscattered electron image analysis of sample MO1108 shows that modal percentage

of magnetite is ~3.8 vol.% (e.g. Figure 5d). Magnetite is thought to be part of the metamorphic paragenesis because of its tendency towards rounded shapes as cordierite inclusions, as well as their homogeneous distribution along with mica in mica-rich (M) domains, showing grain coarsening compared to the inclusion (Figure 5). An important difference between these magnetite-rich rocks and the more common, ilmenite-bearing, reduced metapelites, is that muscovite dominates over biotite with 32 vol.% (Figure 5d) instead of the 11 vol.% modal proportion typical of the reduced metapelites.

3.4 | Sillimanite–K-feldspar zone (samples Mel3, Mel4, Leu4)

The onset of partial melting and the occurrence of first leucosome veins within metapelitic layers are marked by

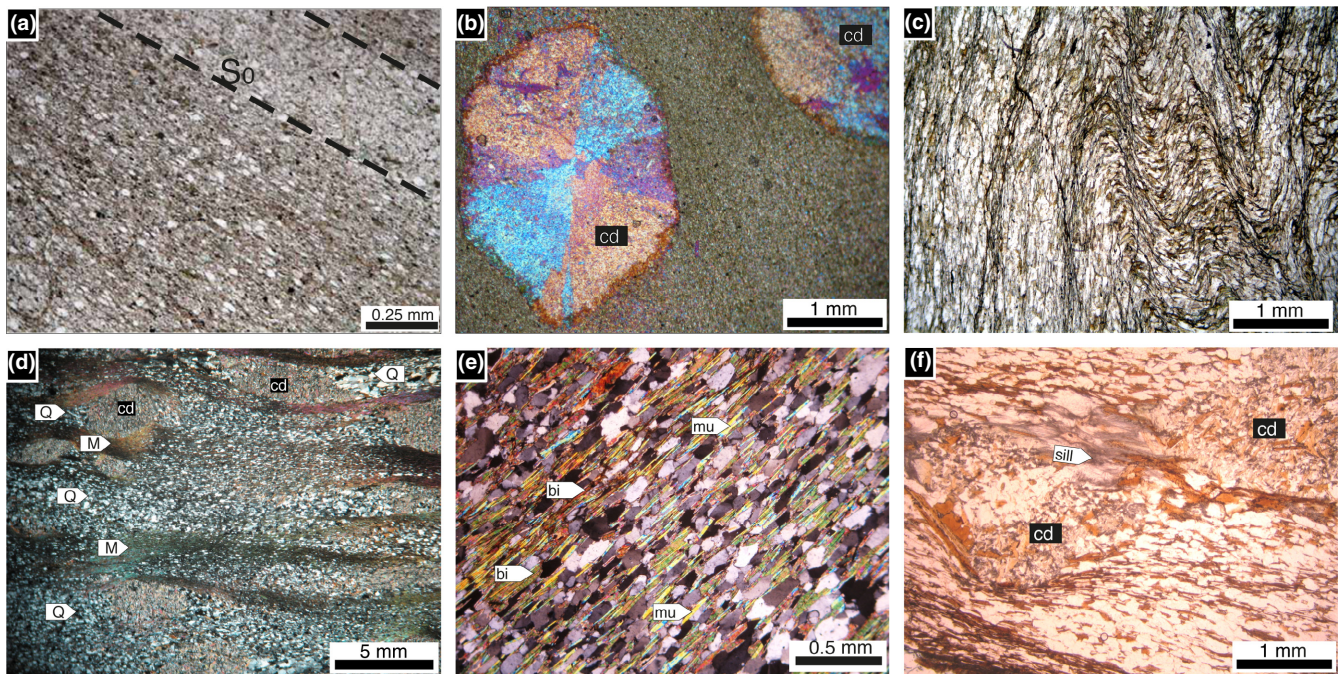


FIGURE 4 Photomicrographs of common microstructural features of metapelites at subsolidus conditions. (a) Layering in a low-grade sample of Puncoviscana Formation from the north side of Sierra de Molinos. Plane-polarized light (PPL). (b) Detail of pseudo-hexagonal cordierite porphyroblast displaying characteristic sector twinning in very fine-grained matrix. One-wave quartz plate inserted to emphasize twinning. (c) Crenulation cleavage in phyllite from the chl–mu zone (PPL). (d) Cordierite-bearing micaschist from the mu–bi zone, showing development of Q (quartz-rich) and M (mica-rich) domains. Elongated cordierite (cd) is replaced by fine-grained mica aggregates. Mica-rich bands are best developed around cd grains. Cross-polarized light (XPL). (e) Detail of matrix in cordierite-bearing micaschist, showing biotite and muscovite in equal proportions (XPL). (f) Cordierite partially replaced by sillimanite (fibrolite) close to contact with sill–ksp zone (PPL)

the disappearance of primary muscovite and appearance of widespread sillimanite and K-feldspar in the mineral assemblage. Migmatitic rocks are subdivided into metatexites and diatexites. Metatexite is defined as a migmatite where the rock did not lose coherence and preserves pre-partial melting structures such as layering. Typically, they mark regions where the melt fraction at any point during anatexis, remained relatively low (Brown, 1973; Sawyer, 2008). The Molinos metatexite migmatites are generally stromatic consisting of numerous thin (commonly 2 mm to 2 cm wide) and laterally persistent bands of light coloured quartzo-feldspathic leucosomes, usually bound by dark biotite-rich melanosomes (Figure 2d). Stromatic metatexites are the most abundant variety of migmatite in the area. Most leucosomes are laterally continuous and parallel to the main foliation and compositional layering, but some of them are located at dilatant sites such as interboudin partitions and small shear bands outlining net-like patterns and cross-cutting the main foliation (Figure 3a–c). The leucosomes located at such dilatant sites are commonly coarser-grained than leucosomes parallel to the foliation. Alternatively, leucosomes may be distributed as irregular patches or lenses. According to their mineral assemblages metatexites were subdivided into two main

groups: the first one containing sillimanite and K-feldspar in the neosome (sill–ksp metatexites), and the second dominated by cordierite and K-feldspar, where sillimanite is scarce or absent (cd–ksp metatexites). The latter are only found in the cd–ksp zone described in the next section. Leucosomes in the sill–ksp metatexites are usually trondhjemitic, composed of quartz, plagioclase, muscovite, tourmaline and rare biotite, with accessory sillimanite or cordierite. In this case the melanocratic host matrix exhibits grano-lepidoblastic schistose texture and has an assemblage of biotite, quartz, fibrolitic sillimanite, K-feldspar (microcline/micropertite), plagioclase with accessory apatite, tourmaline, zircon and monazite (Figure 6a,b). The main foliation is defined by preferred orientation of biotite and sillimanite (Figure 6a). Some of these migmatites contain retrograde, possibly late magmatic, muscovite that grew as skeletal flakes replacing sillimanite and/or K-feldspar (Figure 6b).

Most diatexites in this zone are gray, equigranular, fine-grained rocks consisting of plagioclase, quartz, biotite (<15%), muscovite, sillimanite, apatite and tourmaline. K-feldspar is rare or absent. Biotite is normally distributed uniformly but may locally form biotite- or biotite+sillimanite-rich schlieren that outlines a flow-

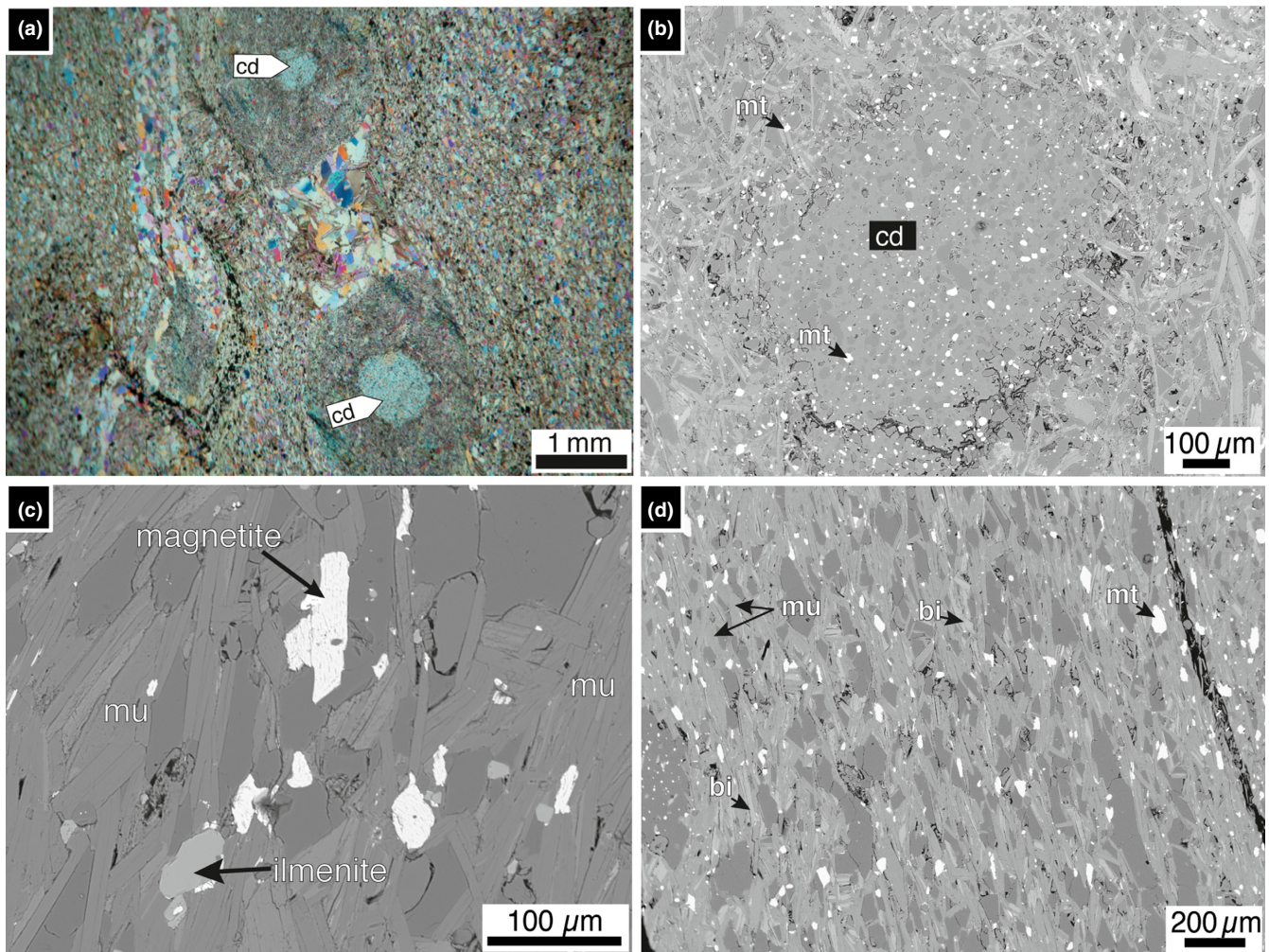


FIGURE 5 Photomicrograph of oxidized micaschist, sample MO1108 (mu–bi zone). (a) Preserved cores of cordierite in porphyroblasts. Note abundance of oxides (opaque material) wrapping around porphyroblasts and as tiny inclusions and crystals of quartz and plagioclase in the pressure shadows linking two porphyroblasts. Quartz plate inserted. (b–d) Back-scattered electron images (BSE). (b) Detail of a cordierite grain (rounded outline) containing numerous magnetite inclusions (light, small and equant grains) homogeneously distributed. Matrix surrounding comprises mica flakes and magnetite in a darker grey interstitial quartz and plagioclase. (c) Magnetite and ilmenite aligned parallel to mica in matrix. (d) Magnetite distributed in a quartz-mica matrix. The modal amount of magnetite measured in this image is 3.82 vol.% measured using the software ImageJ v1.49 (<http://imagej.nih.gov/ij/>). Note also that muscovite dominates over biotite (mu 32%, bi 11%). Biotite in this sample is phlogopitic (see text)

banding or layering in the rock. Sillimanite is prismatic and less abundant than in metatexites.

3.5 | Cordierite–K-feldspar zone (samples ResB, MO1114, MO1113)

The transition between the previous sill–ksp zone and this zone is marked by the appearance of cordierite associated with leucosomes and the abrupt disappearance of sillimanite toward the east. In the cd–ksp metatexites, the leucosomes are composed of quartz, K-feldspar, plagioclase, cordierite, subordinate biotite and apatite. The mesosome and melanosome show grano-lepidoblastic texture

consisting of biotite, K-feldspar, cordierite, plagioclase and quartz. The main foliation is defined by the preferred orientation of biotite. Sillimanite is absent in most samples and its rare occurrence is restricted to minor amounts inside or surrounded by cordierite. Cordierite is abundant (up to 30 vol.%) in metapelitic layers occurring as porphyroblasts of up to 7 cm in size. It encloses small rounded inclusions of biotite, quartz and occasionally sillimanite and tourmaline. Cordierite and K-feldspar poikiloblasts usually develop inclusion-free rims when they are adjacent to leucosomes, whereas inside the melanosome/mesosome they have inclusion-rich areas. These features suggest crystallization from a melt or growth in a melt-rich environment

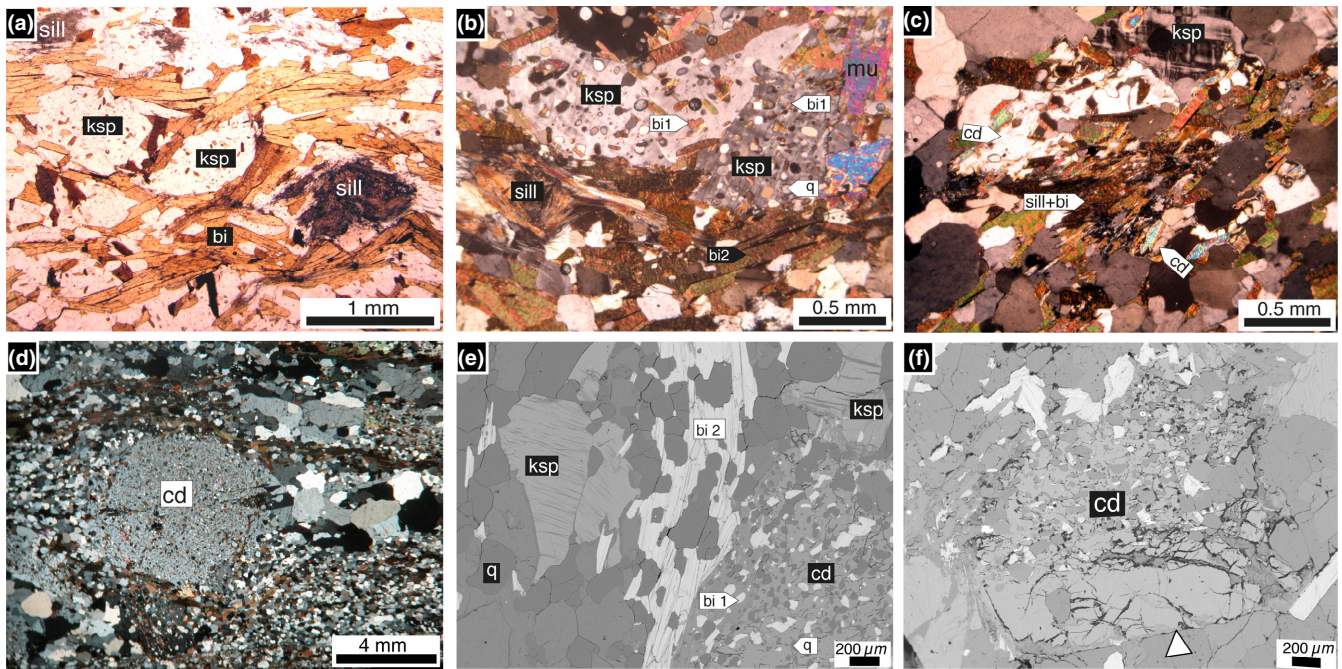


FIGURE 6 Photomicrographs of suprasolidus rocks from Sierra de Molinos. (a) Matrix in metatexite from sill–ksp zone. Foliation is horizontal defined by orientation of biotite which wraps around ksp poikiloblasts. Plane-polarized light (PPL). (b) Matrix in a metatexite surrounding ksp poikiloblasts with rounded/elliptical inclusions of quartz and biotite. At the top right of the photo late mu replacing ksp. Cross-polarized light (XPL). (c) Sillimanite+biotite aggregate surrounded by cordierite. The spatial relationship among minerals suggests a prograde reaction of consumption of biotite and sillimanite to form cordierite. (XPL) (d) Cordierite poikiloblast in leucosome from cd–ksp zone metatexite. Note well-preserved cd with multiple inclusions of small grains of quartz and biotite. (XPL) (e and f) Back-scattered electron (BSE) images. (e) Cordierite poikiloblast with rounded inclusions of biotite and quartz. Note the distinction between the larger grain size of biotite in matrix (bi2). (f) Cordierite porphyroblast with inclusion-rich core and inclusion-free rim (massive region at the bottom) indicating two distinct growth phases. White arrow marks a straight crystal cordierite face, suggesting growth from a melt or in a melt-rich environment. Images (d–f) correspond to cd–ksp metatexites without sillimanite, composed essentially of bi–ksp–cd–pl–q

(Figure 6f; e.g. Vernon, White, & Clarke, 2008). Feldspar and cordierite with straight crystal faces against quartz also indicate crystallization from a liquid or in a melt-rich environment (Figure 6f). Apatite, tourmaline, zircon and monazite are the main accessory phases. Zircon and monazite commonly occur as inclusions in major minerals such as biotite and cordierite. Some metatexite migmatites have small volumes of leucosome and are enriched in mafic minerals, suggesting melt loss (Figure 2e).

Diatexites in this zone are predominantly mesocratic and display granoblastic texture consisting of quartz, biotite, K-feldspar, plagioclase, cordierite, muscovite, with accessory sillimanite, tourmaline and apatite. Biotite does not show a strong preferred orientation and it is generally retrogressed to chlorite. Cordierite forms anhedral to subhedral grains and is usually replaced by fine-grained retrograde aggregates. K-feldspar (microcline) commonly contains numerous round-shaped inclusions of biotite and quartz. Most of the muscovite is assumed to be late and occurs as large flakes replacing sillimanite and biotite or forming symplectite with quartz. Plagioclase and quartz preserve locally polygonal shapes.

4 | MINERAL CHEMISTRY

Chemical analyses of minerals in metapelites from the mu–bi, sill–ksp and cd–ksp zones were conducted on a JEOL JXA-8230 electron microprobe at the University of Brasilia using wavelength-dispersive spectrometry. Operating conditions were 15 kV accelerating voltage and beam current of 10–15 nA, with a beam diameter of 3 μm (for mica and cordierite) and 6 μm (for feldspar). All results were subjected to matrix corrections based on the ZAF (atomic number–absorption–fluorescence) method (Reed, 2005). The magnetite–ilmenite-bearing micaschist sample MO1108 from the mu–bi zone, three metatexite migmatite samples from sill–ksp zone (melanocratic matrix: Mel3, Mel4; leucosome: Leu4) and three metatexite samples from the higher-grade cd–ksp zone (ResB, MO1113, MO1114) were investigated (see Figure 1 for location). More than 100 analyses of biotite and a similar number of cordierite analyses were carried out, while plagioclase, K-feldspar, muscovite and other accessory minerals were analyzed to a lesser extent. The complete electron microprobe mineral chemistry dataset is provided in Table S1.

Plagioclase shows a small compositional range and is mostly oligoclase with limited zoning. In the sill–ksp zone, melanosome plagioclase has An 16–23 while leucosome has An 8–13 with one albite grain analyzed (An 4). In the three samples from the cd–ksp zone, plagioclase has a more restricted composition, An 15–18 and K-feldspar (microcline/microperthite) corresponds to Or 0.82–0.94. Muscovite is only observed as a primary phase in the mu–bi zone with $[\text{Na}/(\text{Na}+\text{K})] = 0.11\text{--}0.16$ and a variable X_{Fe} $[\text{Fe}/(\text{Fe}+\text{Mg})] = 0.50\text{--}0.70$ and Si that ranges from 6.08 to 6.18 atoms per formula unit (a.p.f.u.), based on a 22-oxygen formula.

Biotite in the magnetite–ilmenite-bearing micaschist MO1108, from the mu–bi zone, has $X_{\text{Fe}}(\text{bi}) = 0.25\text{--}0.29$, towards the phlogopitic end-member and Ti a.p.f.u. = 0.10–0.14. This contrasts with biotite in metapelites without magnetite from the sill–ksp zone, which is markedly more ferrous with $X_{\text{Fe}}(\text{bi}) = 0.49\text{--}0.54$. The biotite of the cd–ksp zone was subdivided into two textural groups (Figure 6b, e): (1) Biotite1 (bi1) forms round-shaped inclusions in cordierite or K-feldspar porphyroblasts, and (2) Biotite2 (bi2) is in the matrix, commonly outlining the main foliation (Figure 6e). Biotite in this zone exhibits the highest X_{Fe} values ranging from $X_{\text{Fe}}(\text{bi}) = 0.54\text{--}0.59$ for biotite 1, similar to that for biotite 2, ranging from $X_{\text{Fe}}(\text{bi}) = 0.54\text{--}0.6$.

Metamorphic cordierite in the oxidized micaschist (MO1108) has $X_{\text{Fe}}(\text{cd}) = 0.15\text{--}0.17$ (mean = 0.16; $SD = 0.007$) and is markedly more magnesian than peritectic cordierite in migmatites from the cd–ksp zone with $X_{\text{Fe}}(\text{cd}) = 0.40\text{--}0.48$ (mean = 0.417; $SD = 0.016$). Thus, both biotite and cordierite from the oxidized micaschist (MO1108) are considerably more magnesian than their counterparts in reduced samples.

5 | Ti-IN-BIOTITE GEOTHERMOMETRY

The temperature of metamorphism was estimated using the Ti-in-biotite geothermometer (TIB; Henry, Guidotti, & Thomson, 2005) in metapelites from different metamorphic zones (Figure S1). Henry et al. (2005) suggested that geothermometric calculations based on the amount of Ti and X_{Mg} ratio $[\text{Mg}/(\text{Mg}+\text{Fe})]$ in biotite can be applied to graphitic peraluminous metapelites that contain rutile and/or ilmenite and have equilibrated at ~4–6 kbar and 480–800°C, respectively. The metamorphic rocks from Sierra de Molinos are well within the TIB geothermometer restrictions since they are peraluminous metapelites with mineral assemblages that not only reflect low pressure but also contain ilmenite as the Ti-saturated mineral, and sillimanite and/or cordierite as aluminous phases. Despite the lack of graphite in these metapelites, studies such as Erić, Logar, Milovanović, Babič, and Adnadević (2009) have shown that this method can be successfully applied to non-graphitic metapelites. These authors

compared TIB temperature estimates for non-graphitic metapelitic assemblages against other geothermobarometric methods. They found that the estimates compared favourably in samples where Ti-content showed a negative correlation with X_{Mg} , in agreement with the principle of the TIB method, but found discrepancies of up to 110°C for samples where biotite showed a positive correlation. As biotite in all the samples shows negative correlation between Ti-content and X_{Mg} , we expect that the TIB temperatures are not greatly affected by the absence of graphite. The precision of the thermometer is estimated to be $\pm 24^\circ\text{C}$ at $<600^\circ\text{C}$, improving to $\pm 12^\circ\text{C}$ at $>700^\circ\text{C}$ (Henry et al., 2005).

Mu–bi zone: sample MO1108 is located almost at the boundary with the sill–ksp zone (see Figure 1). It yielded TIB values of 530–597°C (Figure S1a). Although the Ti contents of biotite do not vary substantially (Ti ~0.10 to 0.14 a.p.f.u.), the closely spaced Ti isotherms in magnesian biotite ($X_{\text{Mg}} > 0.7$), yield significant variation of temperature ($SD = 20^\circ\text{C}$).

Sill–ksp zone: In this zone biotite is red-brown and texturally homogeneous. Sample Mel4 yielded TIB values of 594–652°C, almost identical with those calculated for the leucosome (Leu4), 602–647°C. The maximum TIB value of 660°C was obtained for sample Mel3 (Figure S1b).

Cd–ksp zone: Compared with matrix biotite (biotite 2), biotite inclusions (biotite 1) exhibit lower Ti contents suggesting equilibration at lower temperatures. It is possible that biotite inclusions preserve equilibrium attained during prograde metamorphism and did not re-equilibrate at peak conditions as the matrix biotite may have done. This tendency is observed more markedly in sample ResB, where the maximum temperature for matrix biotite was ~700°C, whereas some biotite inclusions yield $<650^\circ\text{C}$ (Figure S1c). In sample MO1113 the average TIB temperatures calculated for biotite inclusions is 675°C ($SD = 18^\circ\text{C}$), whereas for matrix biotite it rises to 686°C ($SD = 16^\circ\text{C}$). In sample MO1114, matrix biotite yielded a maximum temperature of 700°C and once again the average temperature is slightly higher (680°C, $SD = 16^\circ\text{C}$) than the average value for biotite inclusions (675°C, $SD = 21^\circ\text{C}$). The values derived from the Ti-rich matrix biotite are taken to represent the temperatures achieved in the cd–ksp zone approaching a uniform maximum value of ~700°C (Figure S1c). This compares with values between 600 and 660°C for the sill–ksp zone and below 600°C for the mu–bi zone (Figure S1).

6 | PHASE EQUILIBRIA MODELLING

In order to constrain the evolution of the mineral assemblages and the partial melting process, phase equilibria modelling was undertaken using THERMOCALC

v3.33 (Powell & Holland, 1988) and the internally consistent dataset of Holland and Powell (1998; datafile tcds55.txt, created in November 2003). Calculated P - T phase diagrams were contoured for the abundance and composition of phases using TCIInvestigator (Pearce, White, & Gazley, 2015). All the calculations were performed in the system MnO–Na₂O–CaO–K₂O–FeO–MgO–Al₂O₃–SiO₂–H₂O–TiO₂–O (MnNCKFMASHTO) using the following activity-composition models: silicate melt (White, Powell, & Holland, 2007); cordierite (Holland & Powell, 1998; Mahar, Baker, Powell, Holland, & Howell, 1997); biotite, garnet and ilmenite (White, Pomroy, & Powell, 2005); orthopyroxene (White, Powell, & Clarke, 2002), chlorite (Holland & Powell, 1998; Mahar et al., 1997); muscovite (Coggon & Holland, 2002); K-feldspar and plagioclase (Holland & Powell, 2003); epidote (Holland & Powell, 1998) and magnetite (White, Powell, Holland, & Worley, 2000). Additional phases with no solid solution include andalusite, kyanite, sillimanite, quartz and H₂O. Accessory phases containing components outside of the model system MnNCKFMASHTO were not considered for the bulk rock composition calculations. The effects of Mn in pelites is most marked at greenschist to amphibolite facies conditions (e.g. Mahar et al., 1997; Tinkham, Zuluaga, & Stowell, 2001; Wei, Powell, & Clarke, 2004) and is expected to be relevant for the present study.

Although the MnNCKFMASHTO model system is a reasonably realistic analogue for natural metapelitic rocks, additional components that are commonly found in minor quantities, such as F and Zn, may extend the stability of some major phases (e.g. biotite and staurolite). Additionally, the presence of boron in metamorphic fluids, as a consequence of breakdown of detrital tourmaline, may lower the temperature of the wet-solidus and must be considered a possibility given that tourmaline is generally present in the Puncoviscana Formation and its high-grade metamorphic equivalent (Kasemann, Erzinger, & Franz, 2000). Nonetheless, in an experimental study about low-pressure partial melting behaviour of natural boron-bearing metapelites, Spicer, Stevens, and Buick (2004), found that even when tourmaline is clearly a reactant in the partial melting process, it does not appear to shift the fluid-absent incongruent melting reactions markedly. The maximum boron concentration in the melts is attained some 100°C above the solidus. These authors concluded that boron influx into high-grade metasedimentary rocks, for example as a component in an infiltrating fluid phase, at near solidus conditions would result in tourmaline precipitation, not substantial partial melting. At present, we are unable to model such effects thermodynamically.

6.1 | Whole-rock chemistry

For thermodynamic models, a reference composition (MO40_10408) was created to represent the broad mineral changes throughout the metamorphic sequence, as well as samples taken from specific zones: MO1108 (oxidized micaschist from mu–bi zone); Mel3 (metatexite from sill–ksp zone); ResB (metatexite from cd–ksp zone). All compositions used in the calculations, except for sample MO1108, were obtained from XRF analyses presented in Sola et al. (2013). The major element composition of sample MO1108 was obtained from thin section area analysis through integration of several X-ray compositional maps (e.g. Clarke, Daczko, & Nockolds, 2001) using an electron microprobe at Charles University (Prague, Czech Republic). Although this is a very fine-grained homogeneous rock, on the mm to sub-mm scale there is some heterogeneity in the form of fine banding, defined by mica-rich and mica-poor domains. Thus, we integrated such slightly different areas to cover any compositional heterogeneity. Whole-rock compositions used to calculate all pseudosections are given in Table 1.

The reference sample MO40_10408 was obtained by combining the composition of samples MO40 and MO10408 (Figure 1 for location), as suggested by Sola et al. (2013). This reference metapelite corresponds to a subaluminous pelite whose composition is within the typical range of Puncoviscana Formation metapelites (Do Campo & Guevara, 2005). Figure S2 compares the reference metapelite from Sierra de Molinos against Puncoviscana Formation metapelites taken from several localities on a molar proportion basis (Do Campo & Guevara, 2005; 16 samples). Average value for X_{Al} [$Al_2O_3/(Al_2O_3+FeOt+MgO)$] and X_{Ca} [$CaO/(CaO+K_2O+Na_2O)$] for the Puncoviscana Formation is 0.53 and 0.12, respectively, and virtually identical values are found for our reference metapelite with $X_{Al} = 0.52$ and $X_{Ca} = 0.16$.

The relative proportion of ferric to ferrous iron in the sample MO1108 effective bulk composition was increased in order to stabilize the oxide mineralogy, consisting of magnetite+ilmenite in the P - T range of interest, which results in an $X_{Fe^{3+}}$ ($Fe^{3+}/Fe^{3+}+Fe^{2+}$) = 0.49. For a fixed total iron (FeOt) concentration (where $FeOt=FeO+Fe_2O_3$), the conversion of ferrous to ferric iron reduces the available ferrous iron for silicate minerals. The effect of this is that rocks with high Fe_2O_3 concentrations appear more magnesian than their whole-rock FeOt:MgO ratios would suggest (e.g. Boger, White, & Schulte, 2012; Diener & Powell, 2010). For instance, by applying the correction the oxidized sample MO1108 changes drastically its #Mg=[MgO/FeO+MgO] from 0.47 to #Mg=0.63, while in sample MO40_10408 this correction is negligible (from #Mg=0.47 to 0.48).

TABLE 1 Whole-rock compositions used in the construction of pseudosections (molar oxide %)

Sample	Description	Figure	H ₂ O	SiO ₂	Al ₂ O ₃	CaO	MgO	FeO ^{tot*}	K ₂ O	Na ₂ O	TiO ₂	MnO	O
MO40_10408	Puncoviscana Fm (subsolidus)	7a	Excess	68.37	9.62	0.88	4.25	4.69	2.66	2.01	0.50	0.08	0.05
MO1108	Oxidized micaschist (mu–bi zone)	7b,c	Excess	71.73	12.46	0.64	4.59	5.26	3.84	0.78	0.63	0.08	1.30
MO40_10408	Puncoviscana Fm (suprasolidus)	8	5.8	68.37	9.62	0.88	4.25	4.69	2.66	2.01	0.50	0.08	0.05
Mel 3	Metatextite (sill–ksp zone)	9	3.938	68.695	10.323	1.277	4.59	5.099	3.034	2.305	0.595	0.096	0.048
ResB	Metatextite (cd–ksp zone)	10	4.18	65.98	11.42	0.85	5.69	6.26	2.57	2.09	0.63	0.17	0.18
Melt loss	Modelled at 700°C and 4 kbar	11	3.63	69.68	10.13	0.99	4.91	5.40	2.65	1.89	0.58	0.09	0.06
MO40_10408	T–MH ₂ O Puncoviscana Fm	12a X = 0	0	68.37	9.62	0.88	4.25	4.69	2.66	2.01	0.50	0.08	0.05
		12a X = 1	10	68.37	9.62	0.88	4.25	4.69	2.66	2.01	0.50	0.08	0.05
		13 X = 0	4.18	65.98	11.42	0.85	5.69	6.26	2.57	2.09	0.63	0.17	0.18
ResB+melt	T–X _{melt}	13 X = 1	9.54	65.42	10.11	0.65	4.07	4.49	2.63	2.38	0.45	0.12	0.13

*FeO^{tot} is total iron expressed as FeO. O is oxygen, which combines with FeO via the equation 2FeO+O=Fe₂O₃; hence, the amount of O is equal to bulk Fe₂O₃, while true bulk FeO is given by FeO^{tot}–2 × O.

In subsolidus pseudosections (1–6 kbar/500–675°C), all assemblages contain quartz+plagioclase+ilmenite and are considered to be equilibrated in the presence of a pure H₂O supercritical fluid phase.

6.2 | Subsolidus phase equilibria

The observed changes in subsolidus assemblages in Sierra de Molinos metapelites with increasing grade are: chl–bi–mu (chl–mu zone)→bi–mu–cd (mu–bi zone)→bi–mu–sill (top of mu–bi zone). The pseudosection calculated for rock sample MO40_10408 (Figure 7a), indicates that the Sierra de Molinos rocks, lacking garnet, followed a low-*P* path indicated by the arrow. This diagram is dominated by relatively large, high variance ($v = 6$) stability fields. The lowest pressure limit of garnet stability is ~3.1 kbar near 555°C. At higher temperatures, the prograde onset of garnet growth is essentially pressure dependent. Biotite is predicted to be stable in the whole range of pressures and temperatures of Figure 7a. The first major change with temperature is the disappearance of chlorite and simultaneous appearance of cordierite, which is restricted to low pressures above 500°C, represented by the fields: chl–bi–mu & bi–mu–cd (assemblages I and II, Figure 7a). The disappearance of chlorite is temperature-dependent and occurs at ~500–525°C. Andalusite is predicted to be stable in a small region in the centre of Figure 7a (2.8–4 kbar/550–625°C). The molar proportion expected for andalusite is very low <1.5 mol.%. However, fibrolitic sillimanite is recognized instead of andalusite as the Al₂SiO₅ polymorph with grade increase in the mu–bi zone. This discrepancy might be a result of: (1) substantial uncertainties on the andalusite=sillimanite reaction calculated by THERMOCALC (2σ = 30°C), and ii) existence of kinetic barriers that favours fibrolite over andalusite (e.g. Pattison, 1992; Pattison & Tinkham, 2009). Furthermore, the presence of minor elements such as ferric iron in aluminosilicate may shift the equilibria in *P–T* space (e.g. Kerrick & Speer, 1988). In the pseudosection, sillimanite appears for the first time in a narrow field coexisting with cordierite (bi–mu–sill–cd). This reaction is observed in rocks from the mu–bi zone where fibrolite aggregates replace cordierite porphyroblasts (Figure 4f). The assemblage bi–mu–sill (III in Figure 7a) is the commonly observed mineral association before partial melting. Due to the low modal proportion of sillimanite, reflecting the relatively low Al contents of these metapelites, the sillimanite isograd is difficult to identify in the field. The absence of garnet in the Sierra de Molinos metapelite rocks limits the pressure to below 4.8 kbar just before crossing the solidus at 650–660°C, notwithstanding the fact that the first appearance of garnet seems to occur well within garnet-bearing fields, rather than close to the garnet-in conditions due to some degree of overstepping in

the isograd reaction related to kinetic controls (e.g. Carlson, Pattison, & Caddick, 2015; Spear, Thomas, & Hallett, 2014).

Figure 7b is a P – T pseudosection calculated for the oxidized micaschist sample MO1108. Like the previous pseudosection, Figure 7b is dominated by relatively large stability fields in which variance decreases by one ($\nu = 5$) compared to the reference (reduced) sample, due to addition of magnetite to the oxide mineralogy. Garnet and staurolite are not predicted to be stable for this Fe^{3+} -rich composition. Epidote is expected in the high- P –low- T interval and chlorite expands its stability with respect to the reference sample, to higher temperatures at high pressures. In the low- P –high- T portion of the pseudosection, biotite followed by muscovite react to form aluminosilicate and cordierite. The disappearance of biotite before muscovite in this low- P –high- T part of the diagram responds to a higher oxidation state of this sample. High oxidation reduces the available ferrous iron for silicates such as biotite, decreasing its stability at high temperature. The succession of silicate mineralogy from low to high metamorphic grade is similar to the reference metapelite at subsolidus conditions with the main difference being the addition of magnetite: chl–bi–mu–mt \rightarrow bi–mu–cd–mt \rightarrow bi–mu–sill–mt. However, the molar proportion of muscovite is higher than biotite in these oxidized assemblages in accordance with the observed proportion in sample MO1108 (32 modal % of muscovite and 11% of biotite). The observed mineral assemblage and the TIB temperatures obtained for this sample in the mu–bi zone agree with the predicted field: bi–mu–cd–mt located at <4 kbar (Figure 7b). Predicted isopleths for the field bi–mu–cd–mt in Figure 7c reproduce reasonably well the measured compositions [$X_{\text{Fe}}(\text{bi}) = 0.25$ – 0.29 , $\text{Ti}(\text{bi}) = 0.10$ – 0.14 , $X_{\text{Fe}}(\text{cd}) = 0.15$ – 0.17], considering that the model calculations are affected by uncertainties in the end-member thermodynamics and the activity–composition models used.

6.3 | Suprasolidus phase equilibria

Figure 8 shows a P – T pseudosection calculated for the reference metapelite (MO40_10408) that extends from high-grade subsolidus conditions to suprasolidus conditions (1–6 kbar/625–800°C). In Sierra de Molinos primary muscovite is abundant up to and at the migmatite front (Sola et al., 2013). This implies that the regional metamorphic field gradient in Sierra de Molinos passed above the low-variance point “P1” in Figure 8, below which no muscovite should be present. This requires pressures >3.6 kbar at the onset of melting (Johnson, Gibson, Brown, Buick, & Cartwright, 2003; Spear et al., 1999), in accordance with our predictions based on subsolidus paragenesis and shown in Figure 7a (arrow). In this diagram,

the H_2O content was chosen so that the rock is just H_2O -saturated at 4 kbar. As a result, the predicted amount of melt produced by crossing the wet solidus is small <3 mol.% (Figure 8). Beyond the water-saturated solidus, the first major melting reaction encountered is related to the breakdown of muscovite, which produces ~8–9 mol.% of melt over a small temperature interval. At this point the predicted assemblage (bi–sill–ksp–liq) agrees with the observed assemblage for migmatites in the sill–ksp zone (assemblage IV) in which there is an abrupt modal increase of sillimanite and K-feldspar (Figure 6a,b). Likewise, the maximum TIB temperatures obtained for these migmatites (TIB 650–660°C; samples: Mel3, Mel4 & Leu4) are within the range of the predicted assemblage bi–sill–ksp–liq. The microstructures and phase equilibria modelling reveal that cordierite replaces biotite and sillimanite with increasing temperature through the reaction: bi+sill+pl+q \leftrightarrow cd+ksp+liq, represented by the narrow stability field composed by bi–cd–ksp–sill–liq (field V). At peak conditions for cd–ksp zone (TIB ~700°C; samples: ResB, MO1114 & MO1113), sillimanite is consumed and the assemblage in migmatites is dominated by peritectic cordierite and K-feldspar (bi–cd–ksp–liq, assemblage VI in Figure 8). The stability field for this assemblage is limited by the garnet-in line to pressures below 4.3 kbar. The amount of silicate melt predicted for the reference metapelite at peak conditions of 4 kbar and 700°C is ~11–12 mol.% (Figure 8). There is no record of assemblages involving peritectic garnet in equilibrium with cordierite in migmatites from Sierra de Molinos, which marks the transition to granulite facies.

Figures 9 and 10 are pseudosections for sample Mel3 within the sill–ksp zone and sample ResB from the cd–ksp zone, respectively. The water content in these rocks was estimated by means of T – MH_2O diagrams from which we derived the exact amount of H_2O to preserve the chemistry and assemblage at the solidus (see details in Hasalová et al., 2008). The observed assemblage in sample Mel3 corresponds to the small field bi–ksp–sill–liq located near the centre of the diagram (Figure 9). The insets to the right shows the predicted isopleths for biotite $X_{\text{Fe}}(\text{bi}) = 0.51$ and plagioclase $X_{\text{Ca}}(\text{pl}) = 0.23$, that are consistent to those measured in this zone [$X_{\text{Fe}}(\text{bi}) = 0.49$ – 0.51 and An 16–23]. The proportion of phases (mol.%) in this field are: bi 29%, ksp 10%–11%, pl 21%–22%, q 34%, sill 3.5%, liq 0%–0.5%, ilm <1%. The expected temperature for this small field (from 670 to 685°C) is only slightly higher than the TIB thermometry values (660°C, Figure S1b). The final equilibration to preserve the assemblage bi–ksp–sill during cooling is expected to occur between 3.8 and 4.8 kbar.

The observed assemblage in sample ResB corresponds to the relatively large hexavariant field bi–cd–ksp–liq that extends from ~1 to 4 kbar and 655–730°C (Figure 10).

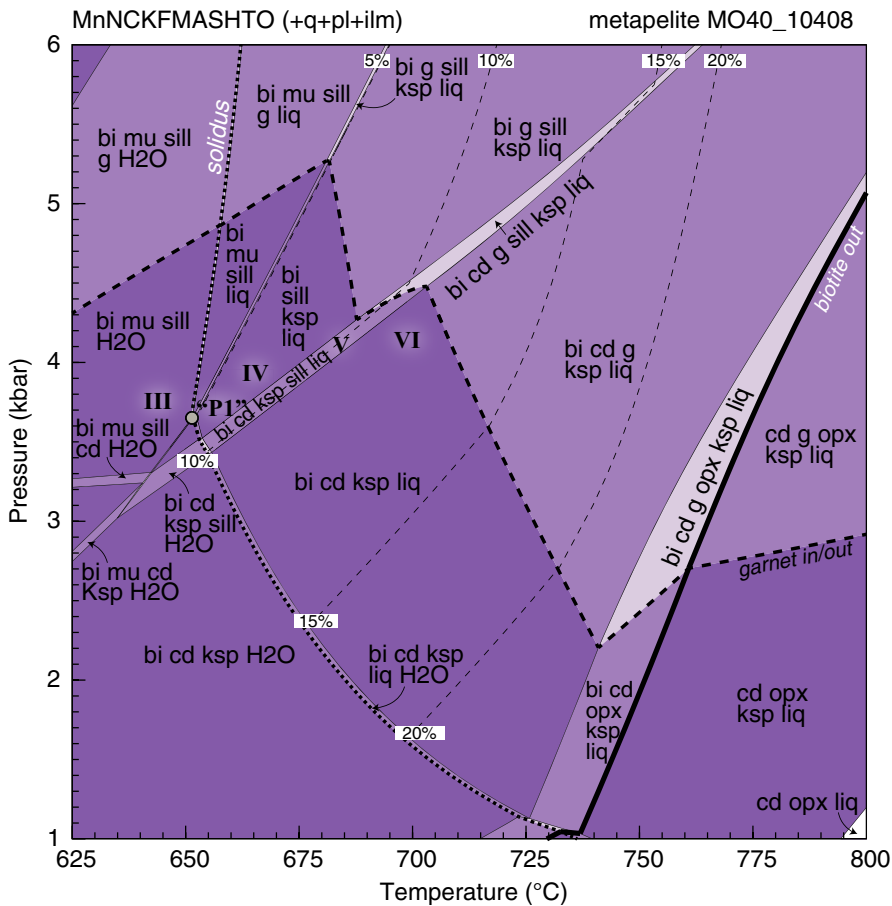


FIGURE 8 Suprasolidus MnNCKFMASHTO P - T pseudosection showing phase relations for the reference metapelite (sample MO40_10408) and melt proportion contours (mol.%) for different fields (narrow dashed lines). Roman numerals correspond to the main assemblage recognized in petrography. Bold dashed line separates fields with garnet, above from those without, below

The modelled composition isopleths for biotite $X_{\text{Fe}}(\text{bi}) = 0.54$, cordierite $X_{\text{Fe}}(\text{cd}) = 0.40$ – 0.41 and plagioclase $X_{\text{Ca}}(\text{pl}) = 0.18$ agree well with the range of measured compositions [$X_{\text{Fe}}(\text{bi}) = 0.56$ – 0.63 , $X_{\text{Fe}}(\text{cd}) = 0.41$ – 0.45 , $X_{\text{Ca}}(\text{pl}) = 0.15$ – 0.17]. Similarly, the TIB thermometry overlaps satisfactorily with the calculated field (Figure S1c). The preservation of peak assemblage allows an estimate of the final equilibration between 3.2 and 4.2 kbar (Figure 10). The low melt fraction predicted in this field illustrates the residual character for this sample.

In summary, the entire path recorded by rocks in Sierra de Molinos marks a low- P path, where peak conditions reached pressures close to 4 kbar at $\sim 700^\circ\text{C}$.

7 | DISCUSSION

7.1 | Melt loss

The well preserved metamorphic peak assemblage in the metatexites from the cd–ksp zone (Figure 6d–f) is consistent with a large proportion of melt being lost, otherwise peak assemblages would have been retrogressed during melt crystallization (Guiraud, Powell, & Rebay, 2001; White & Powell, 2002). Additional evidence of movement and removal of melt from migmatites are (Sola et al.,

2013): (1) abundance of anhydrous/water-poor peritectic minerals (cordierite, K-feldspar or sillimanite) in migmatites, with amounts of leucosomes that are too small to account for these abundances, and (2) leucosomes that have lost melt evidenced by mineralogy and composition (trondhjemitic Ca–Na-rich leucosomes) (e.g. Morfin, Sawyer, & Bandyayera, 2014; Sola et al., 2013; Solar & Brown, 2001). Sola et al. (2013) also determined by means of mass balance that the majority of metatexites exhibit a residual or melt-depleted bulk composition, estimating melt extraction between 0.13 and 0.25 (13–25 wt%).

In order to investigate the phase equilibria at peak and during retrograde conditions, a single melt loss event was modelled at 4 kbar and 700°C in the reference metapelite MO40_10408 (Figure 11). By doing so, we are modelling the residual composition left after extraction of 12 mol.% of melt generated by dehydration of mica from this reference metapelite within the peak stability field (bi–cd–ksp–liq). The result in Figure 11 is similar to the pseudosection calculated for the residual metatexite from cd–ksp zone (sample ResB; Figure 10). Both predict that upon isobaric crystallization of the remaining melt, their peak assemblage is preserved (white arrow): bi–cd–ksp–liq \rightarrow bi–cd–ksp (+q–pl–ilm). However, the major difference between the diagrams of Figures 10 and 11 resides in the phase

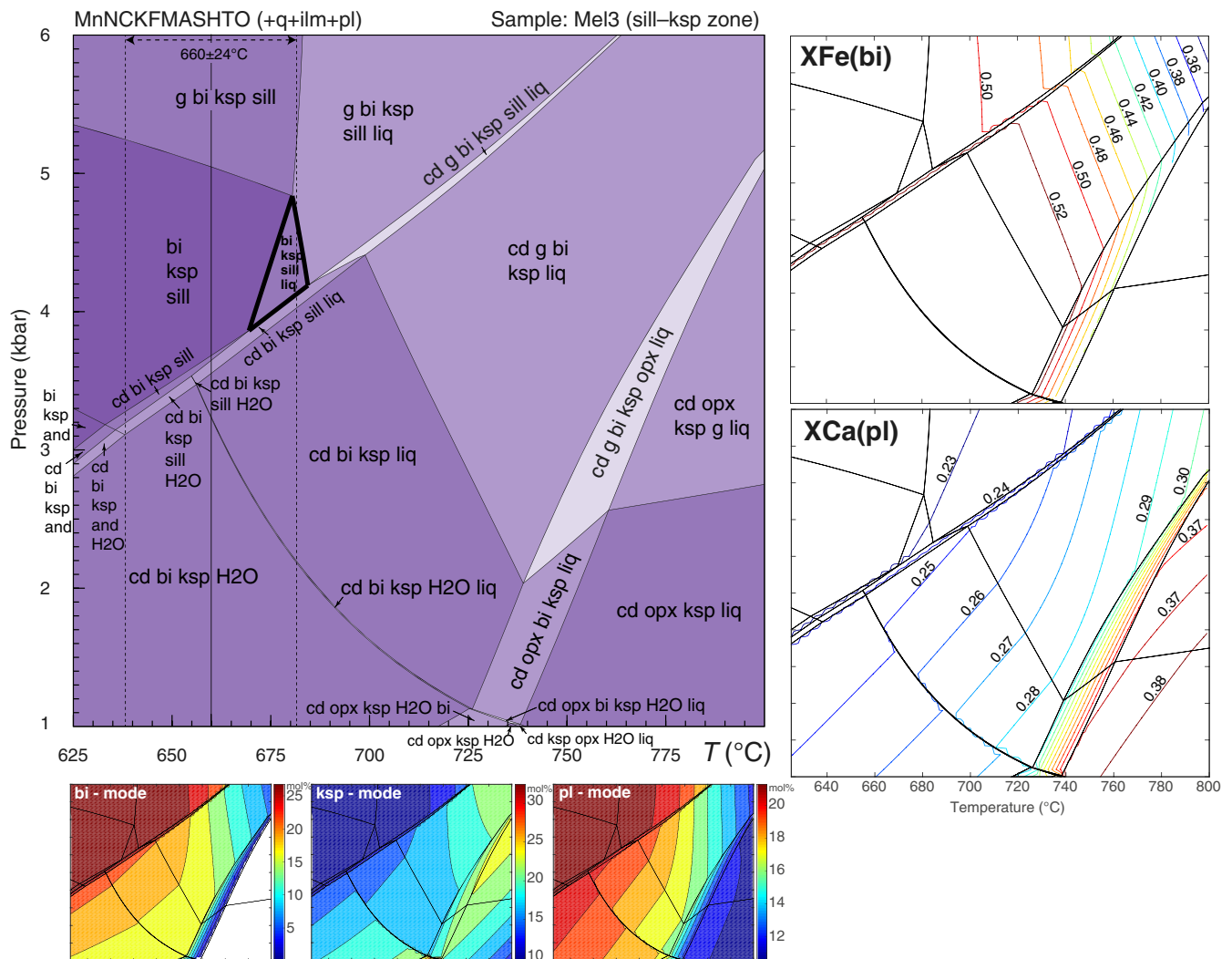


FIGURE 9 P - T pseudosection showing phase relations for sample Mel3 from the sill-ksp zone. Highlighted field corresponds to the observed assemblage in this sample and the vertical lines correspond to the maximum temperature and uncertainties obtained by Ti-in-biotite thermometry. Insets to the right show isopleths for biotite [$X_{\text{Fe}}(\text{bi}) = \text{Fe}/(\text{Fe} + \text{MgO})$] and plagioclase [$X_{\text{Ca}}(\text{pl}) = \text{Ca}/(\text{Ca} + \text{Na} + \text{K})$]. Measured composition: [$X_{\text{Fe}}(\text{bi}) = 0.49$ – 0.51 and An 16–23]. Insets at the bottom show phase proportions (mol.%) for main minerals.

proportions: for the same peak assemblage (bi–cd–ksp–liq), the residual migmatite (sample ResB, Figure 10) contains more cordierite and less quartz and K-feldspar than the modelled residual composition resulting from dehydration melting (Figure 11). For the residual migmatite ResB, upon solidification the diagram of Figure 10 predicts 22 mol.% of cordierite, whereas Figure 11 predicts only 16 mol.%. However, many pelitic rocks in Sierra de Molinos have even more cordierite than sample ResB, suggesting that the correct reference protolith has not been chosen, or we have not quite modelled the system appropriately. One alternative is to investigate whether influx of fluids would increase the modal proportion of peritectic cordierite. The high degree of melt extraction determined by Sola et al. (2013) and the large modal proportion of peritectic cordierite suggest higher degree of partial melting than that

predicted by dehydration melting of the reference protolith. An influx of hydrous fluid during partial melting will enhance melt production (White, Powell, & Holland, 2001; White et al., 2005).

7.2 | Role of water-fluxing

As discussed by Weinberg and Hasalová (2015b), water-fluxed melting can be a common process in nature and its importance is frequently underestimated in the literature. For most cases of water fluxing, there is insufficient water to saturate large rock volumes and so the system is rock buffered, and small amounts of free water may result in voluminous generation of water-undersaturated melts where nominally anhydrous peritectic phases are stable. These are therefore difficult to differentiate from cases of dehydration

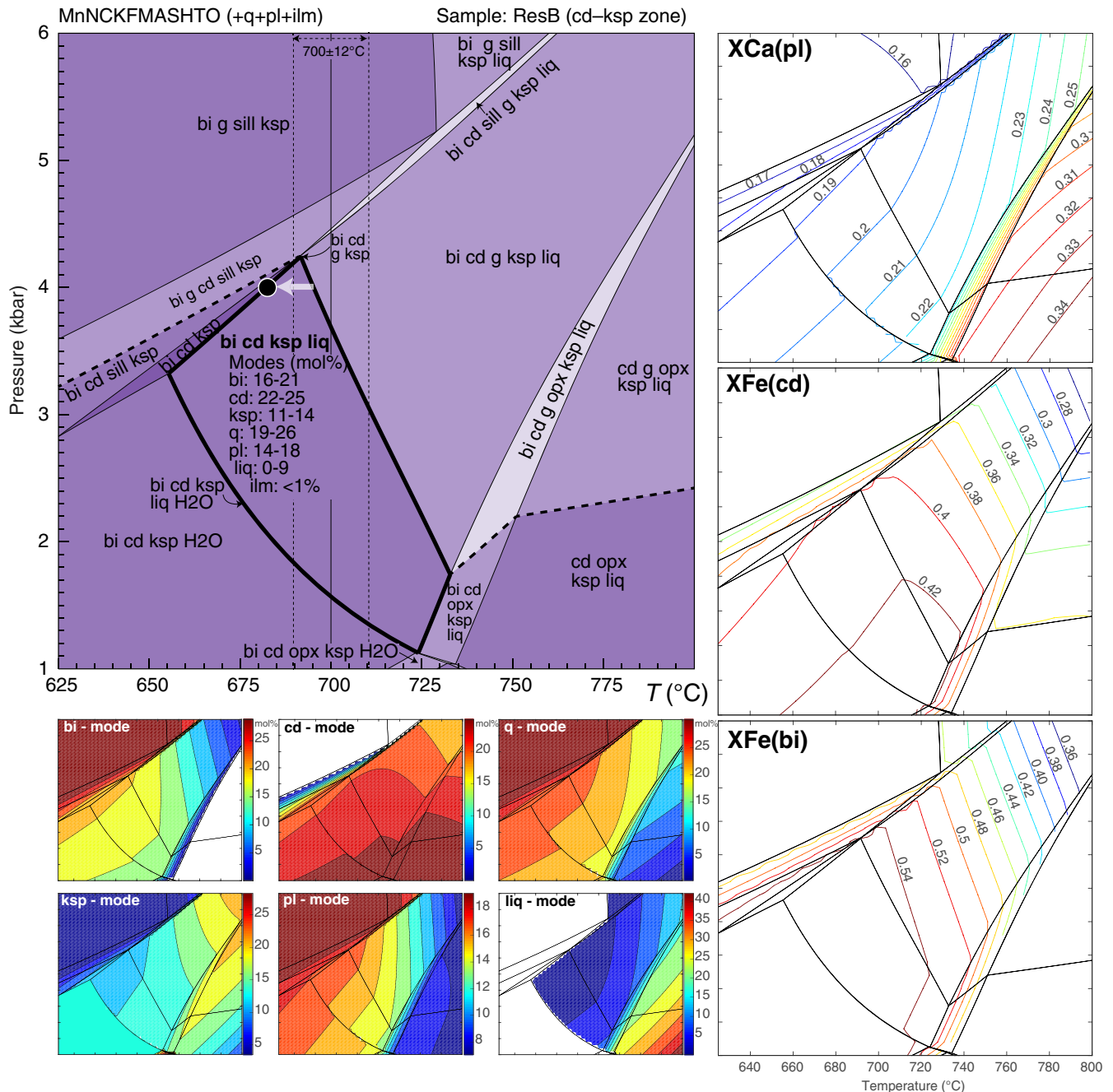


FIGURE 10 P – T pseudosection showing phase relations for sample ResB from the cd–ksp zone. Highlighted field corresponds to the observed assemblage in this sample and the vertical lines correspond to the maximum temperature and uncertainties obtained by Ti-in-biotite thermometry. Insets to the right show isopleths for plagioclase [$X_{\text{Ca}}(\text{pl}) = \text{Ca}/(\text{Ca} + \text{Na} + \text{K})$], cordierite [$X_{\text{Fe}}(\text{cd}) = \text{Fe}/(\text{Fe} + \text{MgO})$] and biotite [$X_{\text{Fe}}(\text{bi}) = \text{Fe}/(\text{Fe} + \text{MgO})$]. Measured composition: [$X_{\text{Fe}}(\text{bi}) = 0.56$ – 0.63 , $X_{\text{Fe}}(\text{cd}) = 0.41$ – 0.45 , An 15–17]. Insets at the bottom show phase proportion (mol.%) for main minerals. The black point at 682 $^{\circ}\text{C}$ and 4 kbar is the melt composition used in the melt reintegration model. See text for explanation.

melting reactions. We show next why the recognition of water-present melting may not be always evident in low- P terranes, and how equilibrium phase diagrams can provide powerful insights about the fluid regime. Since equivalent lithologies can be identified in the field, the reference protolith composition (MO40_10408) is used to investigate different melting scenarios and trends as a function of added H_2O . Having established this theoretical framework,

we then analyze an actual residual rock from the higher-grade zone (sample ResB) and reconstitute its original pelitic composition by adding melt.

To explore the role of water, a T – $M(\text{H}_2\text{O})$ diagram is calculated for the reference protolith composition (Figure 12a). The subsolidus path with increasing temperature for H_2O -saturated assemblages tends to follow the H_2O saturation line, any H_2O generated by dehydration reactions

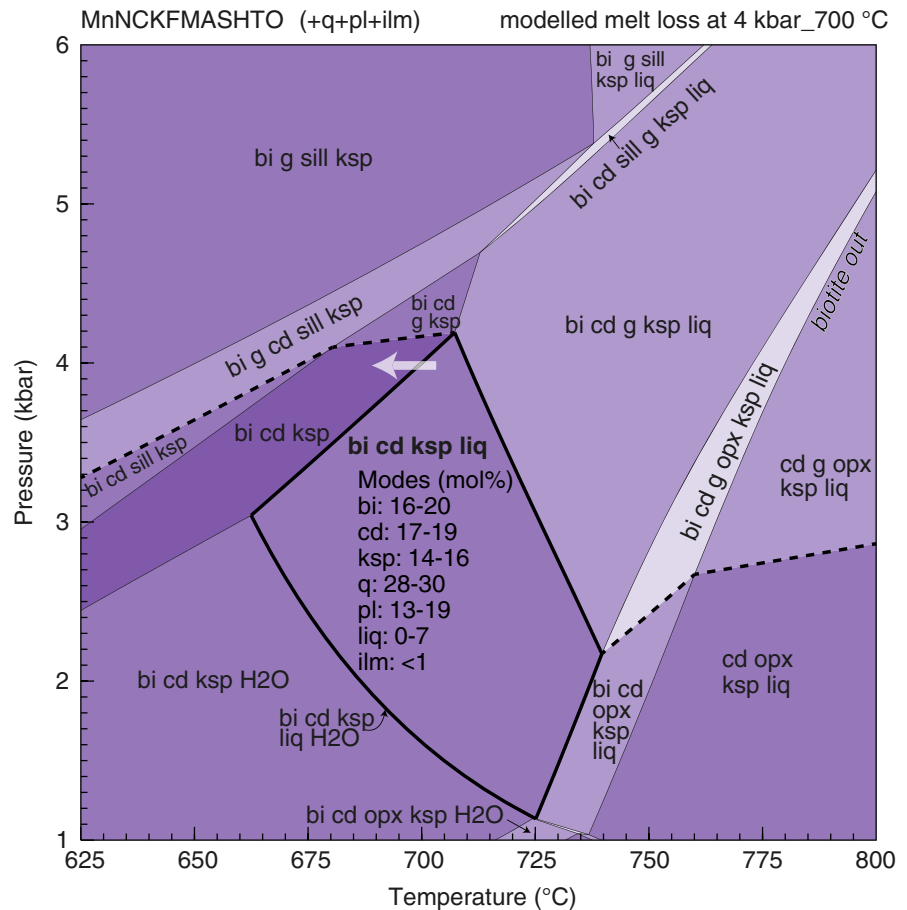


FIGURE 11 P - T pseudosection for a bulk composition formed by removing 12 mol.% melt from a rock with the composition of sample MO40_10408 used in Figure 8, at 700°C and 4 kbar. Notice how this pseudosection is similar to that for ResB in Figure 10. However, the major difference between these two diagrams is phases proportions (see text for explanation). The short white arrow indicates an isobaric cooling to preserve the peak paragenesis upon crystallization (bi-cd-ksp-liq \rightarrow bi-cd-ksp).

being lost from the rock. For closed-system behaviour, the path is vertical above the solidus, as depicted in the figure (path A). When H₂O is added near the solidus, even small amounts have large impact on melt productivity. For path B adding ~2.85 mol.% H₂O, the rock generates over twice the melt (24 mol.%) at the same peak conditions, and for path C adding ~4.5 mol.% of H₂O, melt production is ~30 mol.%.

Another feature of Figure 12a is that, at a given temperature, for example 700°C, the influx of H₂O does not modify the shape of the assemblage fields: the same paragenesis is stable at a range of water contents. This implies that melt extraction from the rock will lead to the same residual mineral paragenesis, though with varied phase proportions such as shown in Figure 12b. The modelled residuum after H₂O-fluxed melting is enriched in cordierite and biotite and depleted in feldspar compared to the residuum left by dehydration melting. In H₂O-fluxed melting less biotite is expected to break down because less structural water is required from hydrous minerals and hence less cordierite should be formed as a peritectic phase. However, quartz, K-feldspar and plagioclase enter in greater proportion in the H₂O-fluxed reaction to form voluminous granitic melt. Similar phase relations for quartz, K-feldspar and plagioclase were determined by Holtz and

Johannes (1991) in low pressure experiments, as a function of H₂O added and melt fraction; where K-feldspar is the first phase to disappear from residuum followed by quartz as the melt fraction and water increase. The extraction of this melt out of the rock results in a melanocratic residuum with a high proportion of ferromagnesian minerals.

On the other hand, no evidence was found that aqueous fluids have a significant impact on the chemistry of solid phases; predicted compositions remain practically unchanged in both dehydration and H₂O-fluxed conditions, and only plagioclase changes towards slightly calcic composition (Figure 12c). This turns problematic the presence of individual peritectic phases or the use of their chemistry to determine the nature of the melting reaction.

7.2.1 | What is the geochemical signature of water-fluxed melting in low- P terranes?

The results above raise the question as to how to determine the nature of the melting reaction in nature. Experimental studies suggest that a large variety of silicate melt compositions can be obtained from melting a similar protolith under variable H₂O contents (e.g. Patiño Douce, 1996; Patiño Douce & Harris, 1998). According to these experiments, the most significant difference between melt

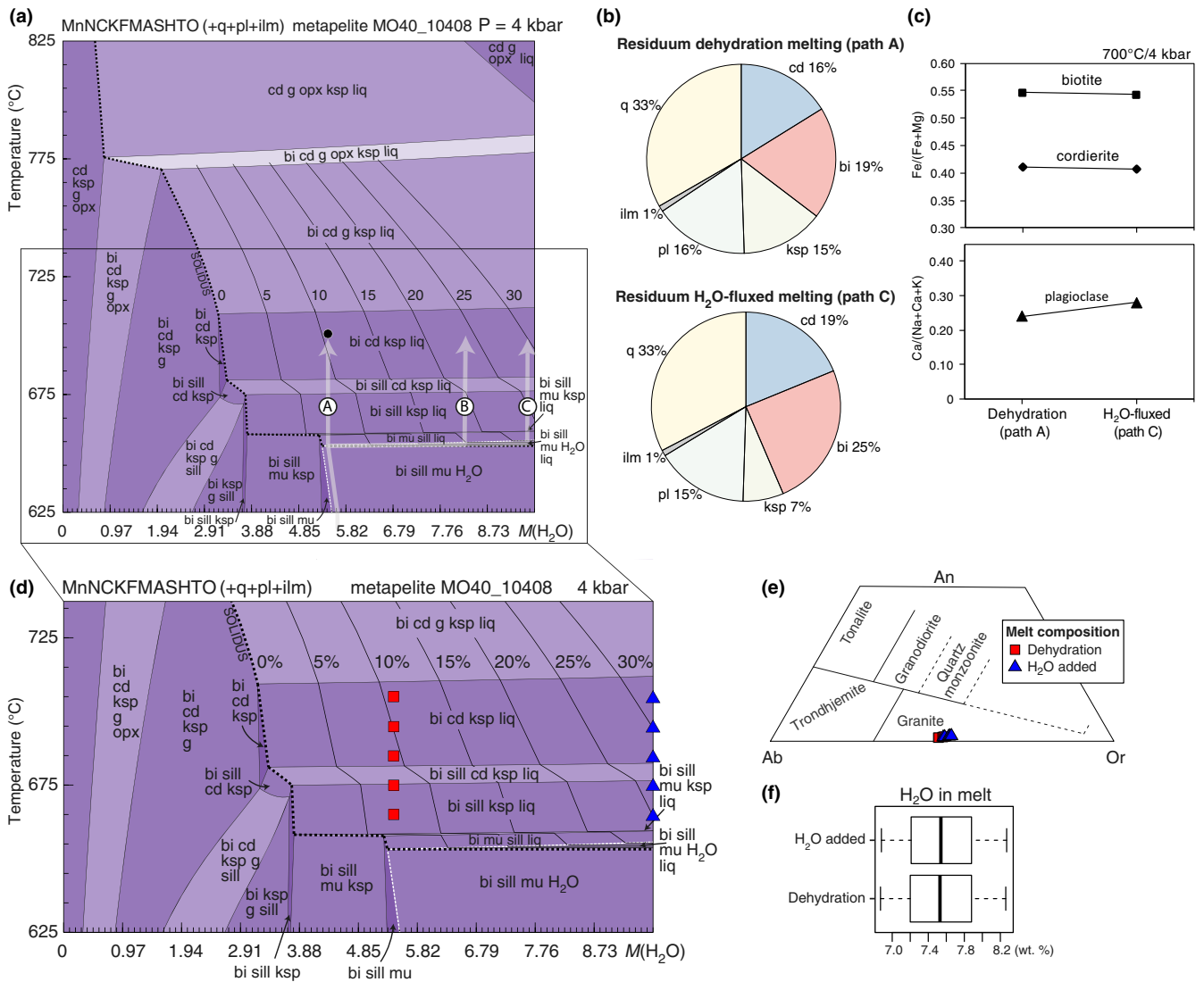


FIGURE 12 (a) T - $M(H_2O)$ pseudosection calculated at 4 kbar for metapelite MO40_10408, including the solidus (black dashed line), H_2O saturation line (white dashed line) and melt mode contours. This phase diagram was used to calculate H_2O content for pseudosection of Figure 8. $M(H_2O)$ represents mol.% of H_2O in the rock. For closed-system behaviour (no H_2O or melt gain/loss), the heating path is vertical once the solidus is crossed (path A). The black point corresponds to peak conditions where closed-system behavior produces 11 mol.% of melt. Hypothetical paths (B and C) assume open-system behaviour with influx of H_2O near the solidus, which shows that even small amounts of water have large impact on melt productivity, more than doubling melt fraction at peak conditions. Notice that the parageneses for these three paths do not change at peak conditions. (b) Modelled residuum left after dehydration (path A) compared to that for H_2O -fluxed (path C) melting at 700°C/4 kbar. The two are generally similar but the latter has 9 mol.% more cordierite+biotite and less feldspar compared to the residuum left by dehydration melting. (c) Impact of aqueous fluids in solid phase compositions. Predicted compositions of ferromagnesian minerals remain essentially constant in both dehydration (path A) and H_2O -fluxed conditions (path C) at 700°C/4 kbar. Plagioclase becomes slightly more calcic composition with the addition of H_2O . (d) Detail of (a) showing points in the prograde path where melt compositions were calculated (Table S5) for dehydration (red squares) and water-fluxed melting (blue triangles). $M(H_2O)$ represents mol.% of H_2O in the rock. (e) Normative An-Ab-Or classification diagram for silicic rocks (O'Connor, 1965) showing composition of melts at conditions indicated in (d). See text for details. (f) Contents of H_2O (wt%) in melts derived from dehydration and H_2O -fluxed reactions showing same values. As per the work of Johannes and Holtz (1996), there is no difference in the water content of the melt as a function of melting reaction since H_2O content is controlled by the minimum amount of water that equilibrates the melt phase. The box represents, for each group, the two quartiles, the line inside is a median, the whiskers denote the overall range

compositions resulting from dehydration melting and water-present melting is the proportion of normative albite, anorthite and orthoclase. For metapelitic protoliths, Patino

Douce and Harris (1998), found that K-rich metasedimentary rocks generated trondhjemitic melts with added H_2O , by contrast to granitic melts produced by dehydration

melting, a tendency observed more markedly in their high- P (10 kbar) experiments than at lower pressure (6 kbar). These authors attributed the trondhjemitic composition of melts in water-added experiments to a decrease in the melting temperature of plagioclase+quartz in the stability field of muscovite, leaving a residuum rich in mica and quartz and depleted in plagioclase. By contrast the same rocks generated granitic melts in experiments without added water, reflecting the breakdown of muscovite. These experimental results contrast with our thermodynamic calculation results at lower pressures (4 kbar, Figure 12; Table S2). The main sources of uncertainty in the experimental approach revolve around whether equilibrium was attained on the scale of the charge and whether the assemblage produced is stable or metastable. In addition, there are uncertainties in the analysis of the phases, compounded by the small grain size and the inherent difficulties in analyzing hydrous and Na-bearing aluminosilicate glasses (White, Stevens, & Johnson, 2011).

The thermodynamic approach allows exploring melt compositions under variable contents of H_2O , where calculations can be done rapidly and easily using the T - M (H_2O) diagram (Figure 12d). First, a H_2O amount is chosen just to saturate the rock at 4 kbar (5.4 mol.% H_2O , red squares) to maximize the structural water contained in mica within the interval from 665 to 705°C. Next, we calculate the composition of melts produced at the same temperature interval with an extra amount of H_2O added (9.7 mol.% H_2O , blue triangles). Melts resulting from water-fluxed reactions display essentially identical chemistry in terms of An–Ab–Or, compared to those resulted from dehydration reactions (Figure 12e; Table S2). Both groups are H_2O -undersaturated melts with similar water (Figure 12f) and ferromagnesian contents (Table S2). The most substantial difference is the proportion of melt produced (Figure 12a), implying that removal of this melt will generate a significantly more melanocratic residuum (Figure 12b) enriched in Al_2O_3 –FeOt–MgO–TiO₂. The similarity in melt composition as a function of water content, in low- T and low- P regimes, implies that melt composition is a poor indicator of the presence of H_2O rich fluids during partial melting. Trondhjemitic plutons, many leucosomes and even various leucocratic diatexites observed in Sierra de Molinos are felsic cumulates resulting from fractional crystallization, rather than water-fluxed melting products, as interpreted by Sola et al. (2013). These cumulates indicate the loss of a fractionated liquid enriched in water, which has the potential to become the water-transport agent as it migrates, potentially triggering more melting in the surroundings.

Whilst the ferromagnesian content of granitic melts is generally very small, experiments also suggest that at constant P - T , MgO and FeO concentrations increase with

increased water content or water activity (Conrad, Nicholls, & Wall, 1988; Holtz & Johannes, 1991; Patiño Douce, 1996). Therefore, melts become apparently more mafic with increasing water content. This contradicts our calculations that predict very similar MgO and FeO concentrations for dehydration and water-present derived melts (Table S2). It is possible that experiments overestimate systematically the melt fraction in water-present runs, causing the melt compositions to shift towards the (more mafic) protolith compositions (see Patiño Douce, 1996). This is because water-present experiments reproduce generally extreme conditions, close to or in excess of the water-saturation solidus (1–8 wt% H_2O added), and the melt fractions for pelitic protoliths might be as high as 80% in such conditions (cf. tables 3 and 4 in Patiño Douce, 1996). Consequently, experiments might not always be appropriate or sensitive enough to assess the effects of subtle changes of free water during partial melting, such as those presented in Figure 12a. Our results yielded granitic melts with very low contents of FeO+MgO, whether or not aqueous fluids were added, and thus variations of natural leucosomes and associated granitoids are interpreted to reflect a combination of residue entrainment and crystal fractionation (see Sola et al., 2013), or different source compositions.

7.3 | Modelled v. actual amount of melt produced by metapelites

The presence of H_2O will promote more voluminous melting compared to water-absent melting, at a given temperature (Figure 12a), and extraction of this melt will change bulk rock composition leaving a residuum enriched in Al_2O_3 –FeOt–MgO–TiO₂ because melts in these conditions do not dissolve appreciable amounts of these elements (Table S2). This is expressed in the increase in cd+bi proportions in the residuum (Figure 12b). Following this reasoning, a residual rock generated by water-fluxed melting will require larger amount of melt to be reintegrated to recover the protolith composition. It is possible, via thermodynamic modelling, to reintegrate melt back into the composition to create an approximate protolith (Bartoli, 2017; Redler, White, & Johnson, 2013; White, Powell, & Halpin, 2004). The fact that melt composition does not vary significantly as a function of melt reaction, water content or melt fraction (Figure 12d–f) means adding melt to the protolith is reasonably straightforward.

Figure 13 shows a T - X pseudosection for a composition range representing mixtures of a residual migmatite (ResB) from cd–ksp zone ($X = 0$) and the same composition + 40% of melt ($X = 1$) formed at 682°C and 4 kbar (black point of Figure 10). It shows that the addition of melt does not affect significantly the solid phase compositions and the temperature boundaries between different fields. The

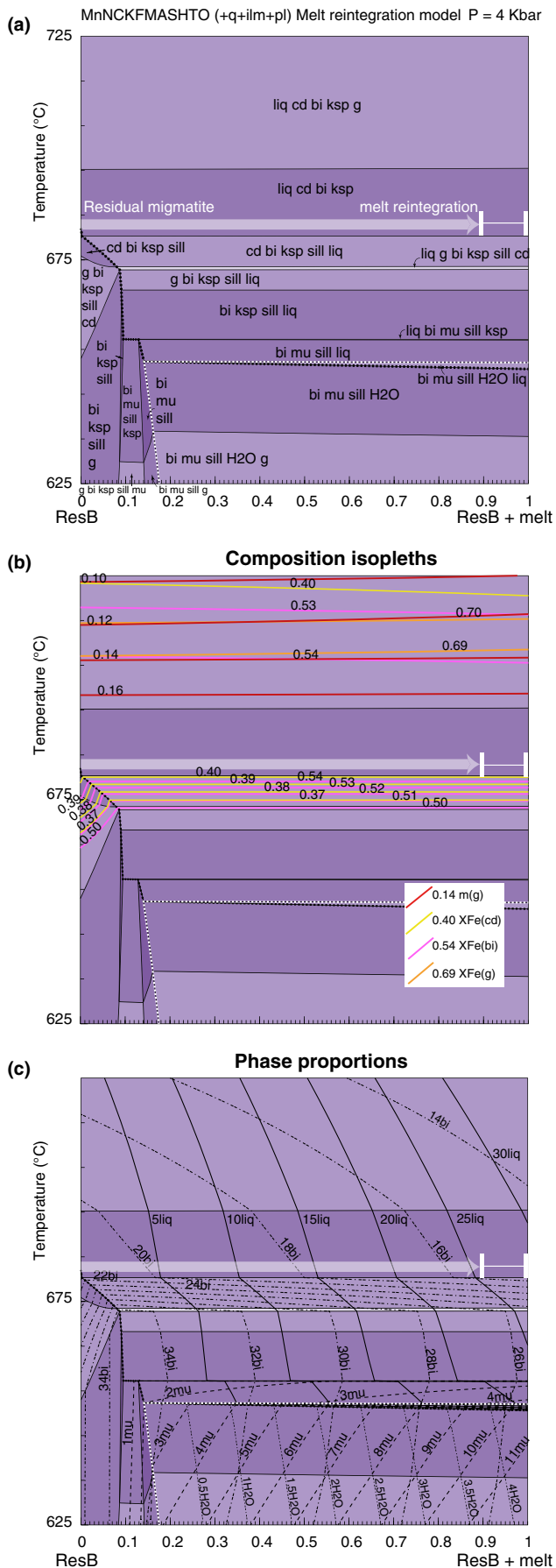


FIGURE 13 (a) T - X pseudosection for a composition range representing mixtures of a residual migmatite (ResB) from cd-ksp zone ($X = 0$) and the same composition + 40% of melt ($X = 1$) formed at 682°C and 4 kbar (black point of Figure 10). The composition of pure melt (wt%) is $\text{H}_2\text{O} = 7.62$, $\text{SiO}_2 = 70.88$, $\text{Al}_2\text{O}_3 = 12.84$, $\text{CaO} = 0.14$, $\text{MgO} = 0.02$, $\text{FeO} = 0.10$, $\text{K}_2\text{O} = 4.83$, $\text{Na}_2\text{O} = 3.57$. (b) Composition isopleths [e.g. $X_{\text{Fe}}(\text{bi}) = \text{Fe}/(\text{Fe} + \text{MgO})$ of biotite; $m(\text{g}) = \text{Mn}/(\text{Fe}^{2+} + \text{Mg} + \text{Ca} + \text{Mn})$ of garnet] and (c) Phase proportions (mol.%) of the main phases

isopleths [$X_{\text{Fe}}(\text{cd})$, $X_{\text{Fe}}(\text{bi})$, $X_{\text{Fe}}(\text{g})$, $m(\text{g})$] remain parallel to the X axis (Figure 13b), and therefore these will not provide clues regarding the proportion of melt that should be reintegrated. By contrast, the phase proportions are strongly influenced by changes in melt fraction (Figure 13c). For the assemblage right before crossing the solidus (bi-mu-sill-H₂O), for example, the ratio between biotite and muscovite (bi/mu) changes drastically from 34/3 = 11.3 for a strongly residual rock ($X \approx 0.2$, Figure 13), to 27/10 = 2.7 for the fertile end-member ($X = 0.9$ to 1). Interestingly, the latter resembles the ratios predicted for the reference protolith where the insets predict 27 mol.% biotite and 10 mol.% muscovite before crossing the solidus at 4 kbar (Figure 7a).

Variations in protolith composition could make impossible to identify the amount of melt that needed to be reintegrated to the residual migmatites to reconstruct the protolith before partial melting. For example, pelites from the Puncoviscana Fm vary in contents of Al_2O_3 (14–20 wt%), SiO_2 (59–71 wt%), Fe_2O_3 (5–7.5 wt%), MgO (1.6–3 wt%), K_2O (2.9–4.8 wt%) (Do Campo & Guevara, 2005). However, these elements do not vary randomly but rather define compositional trends in the protolith that can be used to reconstitute the rock. If the protolith is taken as the sum of two parts: residuum+melt, the best way to evaluate the proportion of each one is by adding melt so as to get the residuum to plot in the main protolith trend. This is shown in Figure 14 where elements that are compatible with the quartz-feldspathic melt (e.g. SiO_2 , K_2O , etc.), are plotted against those compatible with the melanocratic residuum (e.g. Al_2O_3 , FeO , MgO , etc.). Residual rocks plot away from the main trend defined by the compositional range of Puncoviscana pelites. An estimate of how much melt needs to be added can be obtained by adding melt back to the residual rock until its composition reaches the best-fit line. Figure 14 shows that adding melt to the residual composition (X_0), the bulk composition reaches the Puncoviscana protolith at $X = 0.9$ –1, which corresponds to 25–30 mol.% of melt in equilibrium with the bi-cd-ksp-liq field (Figure 13c). This melt fraction is far more than the proportion of melt produced only by dehydration of mica (11 mol.%; Figure 12a), and therefore once again suggests

that melting occurred in the presence of several mol.% of free H₂O.

In summary, we present an approach for reconstituting the protolith by adding melt. This allows estimation of the amount of melt that needs to be added to the residue. We estimate that the residual rock sample requires the addition of more melt than that generated only by (fluid-absent) hydrate-breakdown melting of mica so that excess H₂O needs to be added. In this case an additional 3.5–4 mol.% H₂O (Figure 13) is needed to generate the melt fraction required. Given that peritectic minerals and melt composition are only weakly dependent on the melting reaction, this is a robust way to determine the nature of the melting reaction and the molar proportion of H₂O necessary to account for the melt fraction.

7.4 | Source of aqueous fluids

The amount of free water that can be stored in high-grade terranes is considered to be low. However, there are several mechanisms by which water can be transferred into high-grade crust (refer to Weinberg & Hasalová, 2015b for a review). The most important source of fluid in Sierra de Molinos is interpreted to have been multiple intrusion and crystallization of water-rich magmas (Sola et al., 2013). In this way, melt produced by biotite dehydration melting at depth may be the cause of hydration and melting at shallower crustal levels. A similar interpretation has been proposed to explain melting in metamorphic aureoles (e.g. Finger & Clemens, 1995; Pattison & Harte, 1988; Symmes & Ferry, 1995; Yardley & Barber, 1991). Furthermore, melts generated either by dehydration or water-present melting are H₂O-

rich containing >21 mol.% of H₂O (Table S2) and the release of only a small fraction of this water during crystal fractionation (see Morfin et al., 2014), is sufficient to trigger water-present melting elsewhere (Figure 12a).

7.5 | *P–T* path and regional implications

Pseudosections combined with TIB geothermometry provide improved estimates of the *P–T* conditions of the metamorphic field gradient at Sierra de Molinos. Partial melting at low-pressure conditions described here (Figure 15), reflects perturbed crustal geotherms. In many worldwide examples, low-*P* terranes preserve evidence of a pronounced lateral thermal gradient outward from a high-grade core. Such rocks have commonly been referred to as regional aureoles (White, Chappell, & Cleary, 1974). However, a discrete heat source is not always exposed at the surface. The *P–T* path determined for the study area in Figure 15 supports this interpretation. At such low pressure, the gap between the water-saturated solidus and muscovite-dehydration reaction is very small, and in effect the appearance of melt and disappearance of muscovite occur effectively at the same temperature (Figure 15b) and is not easily recognized in the field.

The trajectory inferred from the isochemical phase diagrams and the sequence of mineral assemblage changes in the rocks from Sierra de Molinos, can be explained by a single metamorphic episode: starting after the protolith deposition at 541–523 Ma (Adams et al., 2008; Sola et al., 2013) with the peak *c.* 470 Ma (Sola et al., 2013).

The migmatites from the study area and nearby regions (Büttner et al., 2005; de los Hoyos et al., 2011;

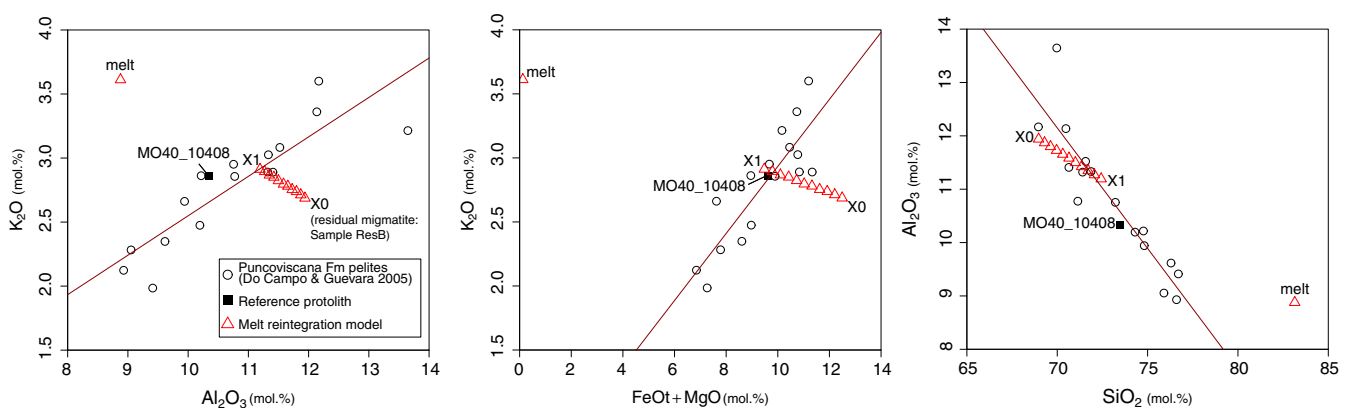


FIGURE 14 Variation diagrams showing the compositional best-fit trend defined by Puncoviscana pelites (from Do Campo & Guevara, 2005). The local reference metapelite MO40_10408 also falls within this line. The composition of the protolith of a residual rock can be estimated by adding melt until its bulk composition reaches the best-fit trend line. Calculations start from a residual composition marked by X0 (corresponding to sample ResB). The composition of the melt is also shown by the isolated triangle in all three plots. The results are consistent with $X = 0.9–1$, which correspond to 25–30 mol.% of melt in equilibrium with the bi–cd–ksp–liq (Figure 13). This compares with 11 mol.% melt produced by dehydration melting (Figure 12a). All data were recalculated to 100 mol.% for SiO₂, TiO₂, Al₂O₃, FeOt, MnO, MgO, CaO, Na₂O and K₂O

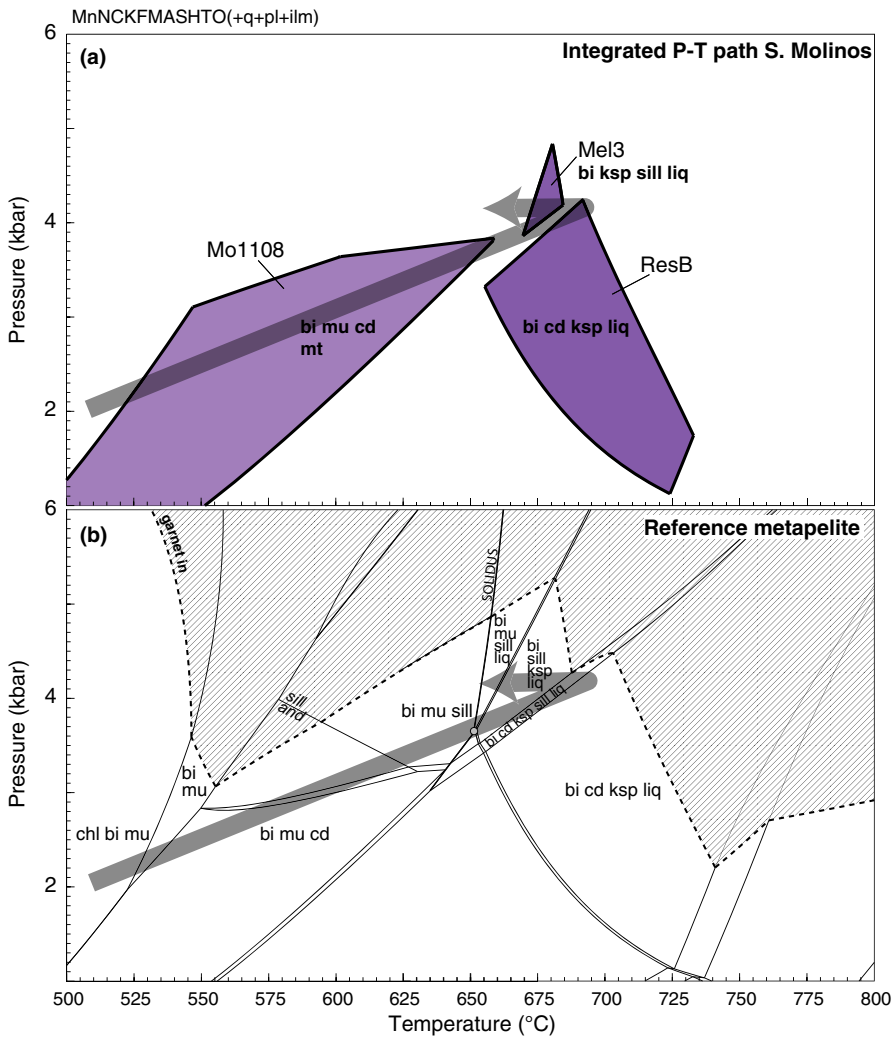


FIGURE 15 (a) Integrated P - T path inferred for Sierra de Molinos rocks based on Figures 7b, 9 and 10. (b) P - T path projected for the reference metapelite MO40_10408

Larovere et al., 2011; Otamendi, Tibaldi, Vujovich, & Viñao, 2008) represent a heated and thermally-weakened backarc, middle to upper crust. Widespread migmatization and magmatism in the Famatinian crust requires high heat input over a great crustal area. Hyndman, Currie, and Mazzotti (2005) argued for an extensive zone of high heat flow in backarcs due to lithosphere thinning over a wide region, independently of whether it is undergoing shortening or extension (Currie & Hyndman, 2006). Backarcs can also be regions of intensive mantle magmatism that increases high heat flux causing low- P /high- T metamorphism. Once the crust starts to melt, melt migration can further influence the thermal structure through heat advection. Such migration will also transfer aqueous fluids further up the crust, leading to more extensive anatexis, driving crustal differentiation as well as weakening of the crust. Periodic fluid influx may lead to multiple melting episodes during a single metamorphic event and therefore will also promote protracted high temperature histories in the continental crust (Rubatto, Hermann, Berger, & Engi, 2009).

8 | SUMMARY AND CONCLUSIONS

In Sierra de Molinos, pelitic rocks preserve evidence of a pronounced lateral thermal gradient with mineral assemblages ranging from greenschist to upper amphibolite facies suprasolidus conditions, defining a low- P /high- T path peaking at 700°C and 4 kbar in the cd-ksp migmatites. Leucosomes at structurally controlled sites such as shear bands, interboudin partitions or network structures, indicate that partial melting and flow occurred under conditions of differential stress during deformation, promoting migration of the melt beyond grain scale producing residual metatexites. The presence of cordierite associated with leucosomes within the higher grade migmatites indicates that melting occurred by incongruent breakdown of biotite. However, significant breakdown of biotite and voluminous melting are not expected at such low- T conditions. Moreover, within suprasolidus domains, metapelitic rocks are rich in ferromagnesian minerals indicating depletion in granitic components with respect to the protolith, implying that they have lost a significant amount of melt. This is

inconsistent with phase equilibria modelling that predicts that only 11 mol.% of melt could have been generated by dehydration of mica. Based on a residual rock, it is calculated that adding nearly 30 mol.% of melt is required to reconstitute it to the protolith composition. This can only be accounted for by adding 3.5–4 mol.% of H₂O during melting. These calculations match independent estimates based on mass balance of major and trace elements (Sola et al., 2013).

Thermodynamic calculations show how small amounts of added free H₂O may increase significantly the melt fraction with little or no change in melt or residual phase composition (Figure 12). Calculations indicate negligible difference in normative An–Ab–Or proportions and ferromagnesian contents between melts derived by dehydration- and water-fluxed melts. The same is true for the content of H₂O in melt, as expected from the diagrams in Johannes and Holtz (1996).

The fact that granitic melts are similar and our models do not predict significant variation in the chemistry of peritectic phases resulting from the addition of small proportion of H₂O (Figure 12e), imply that the presence of fluids during anatexis may not always be recognizable, as also argued by Weinberg and Hasalová (2015b). The most significant change related to water-fluxing is the relative proportions of minerals and the melt fraction, rather than the actual mineral assemblage. Since water-fluxed melts that are undersaturated in H₂O are also mobile, the migration of this extra volume of melt influences whole-rock chemistry of residual rocks. We have developed a simple way based on equilibrium phase diagrams and binary geochemical variation plots, to estimate how much melt a residual rock has lost, if the compositional trends of the protoliths are known.

Our results show how small volumes of water have a significant impact in rock fertility at relatively low temperatures without leaving a trace in terms of the peritectic minerals produced. These findings provide future research lines to be explored and a new perspective on the way H₂O fluxing can occur in nature and the influence of aqueous fluids in crustal anatexis.

ACKNOWLEDGEMENTS

We thank E. Sawyer and R. Palin for their thorough and insightful reviews which substantially improved this manuscript. J. Diener and M. Caddick are also thanked for fruitful discussion and critical revision of an earlier version of the manuscript. M. Brown is thanked for careful editorial handling. This study represents part of the first author's PhD research, funded by the Consejo Nacional de Investigaciones Científicas y Técnicas (CONICET), at the Universidad Nacional de Salta, Argentina. Financial support was

provided by project PICT 2014-3507 (ANPCyT - FonCyT).

REFERENCES

- Aceñolaza, F. G., Miller, H., & Toselli, A. J. (1988). The Puncoviscana Formation (Late Precambrian–Early Cambrian) – sedimentology, tectonometamorphic history and age of the oldest rocks of NW Argentina. In H. Balburg, C. Breikreuz & P. Giese (Eds.), *The Southern Central Andes, Lecture Notes in Earth Sciences* (vol. 17). Berlin: Springer-Verlag.
- Aceñolaza, F. G., Miller, H., & Toselli, A. J. (2000). The Pampean and Famatinian cycles – Superposed orogenic events in West Gondwana. Geoscientific Cooperation with Latin America, Zeitschrift Für Angewandte Geologie Sonderheft SH1, 31^o International Geological Congress, 337–344.
- Adams, C. J., Miller, H., Toselli, A. J., & Griffin, W. L. (2008). The Puncoviscana Formation of northwest Argentina: U-Pb geochronology of detrital zircons and Rb-Sr metamorphic ages and their bearing on its stratigraphic age, sediment provenance and tectonic setting. *Neues Jahrbuch Fur Geologie Und Palaeontologie – Abhandlungen*, 247, 341–352.
- Bahlburg, H., Berndt, J., & Gerdes, A. (2016). The ages and tectonic setting of the Faja Eruptiva de la Puna Oriental, Ordovician, NW Argentina. *Lithos*, 256–257, 41–54.
- Bartoli, O. (2017). Phase equilibria modelling of residual migmatites and granulites: An evaluation of the melt-reintegration approach. *Journal of Metamorphic Geology*, 35, 919–942.
- Becchio, R., Lucassen, F., Kasemann, S., Franz, G., & Viramonte, J. (1999). Geochemistry and isotope systematics of Early Paleozoic metamorphic rocks. Northwest Argentina and North Chile (21°–27°S). *Acta Geologica Hispanica*, 34, 273–299.
- Boger, S. D., White, R. W., & Schulte, B. (2012). The importance of iron speciation (Fe +2/Fe +3) in determining mineral assemblages: An example from the high-grade aluminous metapelites of southeastern Madagascar. *Journal of Metamorphic Geology*, 30, 997–1018.
- Bons, P. D., Druguet, E., Castaño, L. M., & Elburg, M. A. (2008). Finding what is now not there anymore: Recognizing missing fluid and magma volumes. *Geology*, 36, 851–854.
- Brown, M. (1973). The definition of metatexis, diatexis and migmatite. *Proceedings of the Geologists' Association*, 84, 371–382.
- Brown, M. (1994). The generation, segregation, ascent and emplacement of granite magma: The migmatite-to-crustally-derived granite connection in thickened orogens. *Earth Science Reviews*, 36, 83–130.
- Brown, M. (2013). Granite: From genesis to emplacement. *Bulletin of the Geological Society of America*, 125, 1079–1113.
- Büttner, S. H., Glodny, J., Lucassen, F., Wemmer, K., Erdmann, S., Handler, R., & Franz, G. (2005). Ordovician metamorphism and plutonism in the Sierra de Quilmes metamorphic complex: Implications for the tectonic setting of the northern Sierras Pampeanas (NW Argentina). *Lithos*, 83, 143–181.
- Carlson, W. D., Pattison, D. R. M., & Caddick, M. J. (2015). Beyond the equilibrium paradigm: How consideration of kinetics enhances metamorphic interpretation. *American Mineralogist*, 100, 1659–1667.
- Carrera, N., Muñoz, J. A., Sàbat, F., Mon, R., & Roca, E. (2006). The role of inversion tectonics in the structure of the Cordillera

- Oriental (NW Argentinean Andes). *Journal of Structural Geology*, 28, 1921–1932.
- Clarke, G. L., Daczko, N. R., & Nockolds, C. (2001). A method for applying matrix corrections to X-ray intensity maps using the Bence-Albee algorithm and Matlab. *Journal of Metamorphic Geology*, 19, 635–644.
- Clemens, J., & Droop, G. T. (1998). Fluids, P-T paths and the fates of anatectic melts in the Earth's crust. *Lithos*, 44, 21–36.
- Coggon, R., & Holland, T. J. B. (2002). Mixing properties of phengitic micas and revised garnet-phengite thermobarometers. *Journal of Metamorphic Geology*, 20, 683–696.
- Conrad, W. K., Nicholls, I. A., & Wall, V. J. (1988). Water-saturated and undersaturated melting of metaluminous and peraluminous crustal composition at 10 kb: Evidence for the origin of silicic magmas in the Taupo Volcanic Zone, New Zealand, and other occurrences. *Journal of Petrology*, 29, 765–803.
- Currie, C. A., & Hyndman, R. D. (2006). The thermal structure of subduction zone back arcs. *Journal of Geophysical Research*, 111, B08404.
- Diener, J. F. A., & Powell, R. (2010). Influence of ferric iron on the stability of mineral assemblages. *Journal of Metamorphic Geology*, 28, 599–613.
- Do Campo, M., & Guevara, S. R. (2005). Provenance analysis and tectonic setting of late Neoproterozoic metasedimentary successions in NW Argentina. *Journal of South American Earth Sciences*, 19, 143–153.
- Erić, S., Logar, M., Milovanović, D., Babič, D., & Adnađević, B. (2009). Ti-in-biotite geothermometry in non-graphitic, peraluminous metapelites from Crni Vrh and Resavski Humovi (Central Serbia). *Geologica Carpathica*, 60, 3–14.
- Finch, M. A., Weinberg, R. F., Fuentes, M. G., Hasalová, P., & Becchio, R. (2015). One kilometre-thick ultramylonite, Sierra de Quilmes, Sierras Pampeanas, NW Argentina. *Journal of Structural Geology*, 72, 33–54.
- Finger, F., & Clemens, J. D. (1995). Migmatization and “secondary” granitic magmas: Effects of emplacement and crystallization of “primary” granitoids in Southern Bohemia, Austria. *Contributions to Mineralogy and Petrology*, 120, 311–326.
- Genier, F., Bussy, F., Epard, J. L., & Baumgartner, L. (2008). Water-assisted migmatization of metagraywackes in a Variscan shear zone, Aiguilles-Rouges massif, western Alps. *Lithos*, 102, 575–597.
- Guiraud, M., Powell, R., & Rebay, G. (2001). H₂O in metamorphism and unexpected behaviour in the preservation of metamorphic mineral assemblages. *Journal of Metamorphic Geology*, 19, 445–454.
- Hasalová, P., Štípská, P., Powell, R., Schulmann, K., Janoušek, V., & Lexa, O. (2008). Transforming mylonitic metagranite by open-system interactions during melt flow. *Journal of Metamorphic Geology*, 26, 55–80.
- Henry, D. J., Guidotti, C. V., & Thomson, J. A. (2005). The Ti-saturation surface for low-to-medium pressure metapelitic biotites: Implications for geothermometry and Ti-substitution mechanisms. *American Mineralogist*, 90, 316–328.
- Hippert, J. F. F., & Hongn, F. D. D. (1998). Deformation mechanisms in the mylonite/ultramylonite transition. *Journal of Structural Geology*, 20, 1435–1448.
- Holland, T. J. B., & Powell, R. (1998). An internally consistent thermodynamic data set for phases of petrological interest. *Journal of Metamorphic Geology*, 16, 309–343.
- Holland, T., & Powell, R. (2003). Activity-compositions relations for phases in petrological calculations: An asymmetric multicomponent formulation. *Contributions to Mineralogy and Petrology*, 145, 492–501.
- Holtz, F. O., & Johannes, W. (1991). Genesis of peraluminous granites I. Experimental investigation of melt compositions at 3 and 5 kb and various H₂O activities. *Journal of Petrology*, 32, 935–958.
- Hongn, F. D., & Becchio, R. A. (1999). Las fajas miloníticas de Brealito, Valles Calchaquies, Salta. The Brealito mylonitic belt, Calchaquies Valleys, Salta. *Revista de la Asociación Geológica Argentina*, 54, 74–87.
- Hongn, F., Mon, R., Cuevas, J., & Tubia, J. M. (1996). High-temperature caledonian shear zones in the Quebrada Barranquilla (eastern Puna, Argentina): Structural and kinematic outlines. *Comptes Rendus de l'Académie des Sciences Serie Ii Fascicule a-Sciences de la Terre et des Planetes*, 323, 809–815.
- Hongn, F., Mon, R., Petrinovic, I., del Papa, C., & Powell, J. (2010). Inversión y reactivación tectónicas cretácico-cenozoicas en el noroeste argentino: Influencia de las heterogeneidades del basamento neoproterozoico-paleozoico inferior. *Revista de la Asociación Geológica Argentina*, 66, 38–53.
- Hongn, F., Tubía, J., Esteban, J., Aranguren, A., Vegas, N., Sergeev, S., ... Basei, M. (2014). The Sierra de Cachi (Salta, NW Argentina): geological evidence about a Famatinian retro-arc at mid crustal levels. *Journal of Iberian Geology*, 40, 225–240.
- de los Hoyos, C. R., Willner, A. P., Larovere, M. A., Rossi, J. N., Toselli, A. J., & Basei, M. A. S. (2011). Tectonothermal evolution and exhumation history of the Paleozoic Proto-Andean Gondwana margin crust: The Famatinian Belt in NW Argentina. *Gondwana Research*, 20, 309–324.
- Hyndman, R. D., Currie, C. A., & Mazzotti, S. P. (2005). Subduction zone backarcs, mobile belts, and orogenic heat. *GSA Today*, 15, 4–10.
- Insel, N., Grove, M., Haschke, M., Barnes, J. B., Schmitt, A. K., & Strecker, M. R. (2012). Paleozoic to early Cenozoic cooling and exhumation of the basement underlying the eastern Puna plateau margin prior to plateau growth. *Tectonics*, 31, TC6006, doi:10.1029/2012TC003168.
- Jamieson, R. A., Unsworth, M. J., Harris, N. B. W., Rosenberg, C. L., & Schulmann, K. (2011). Crustal melting and the flow of mountains. *Elements*, 7, 253–260.
- Jêzek, P. (1990). Análisis sedimentológico de la Formación Puncovicana entre Tucumán y Salta. *El Ciclo Pampeano En El Noroeste Argentino, Serie Correlación Geológica*, 4, 9–36.
- Johannes, W., & Holtz, F. (1996). *Petrogenesis and experimental petrology of granitic rocks* (Vol. 22). Berlin, Heidelberg: Springer Berlin Heidelberg. <https://doi.org/10.1007/978-3-642-61049-3>
- Johnson, T. E., Gibson, R. L., Brown, M., Buick, I. S., & Cartwright, I. (2003). Partial melting of metapelitic rocks beneath the Bushveld Complex, South Africa. *Journal of Petrology*, 44, 789–813.
- Jung, S., Hoernes, S., & Mezger, K. (2000). Geochronology and petrology of migmatites from the Proterozoic Damara Belt – Importance of episodic fluid-present disequilibrium melting and consequences for granite petrology. *Lithos*, 51, 153–179.
- Jung, C., Jung, S., Nebel, O., Hellebrand, E., Masberg, P., & Hoffer, E. (2009). Fluid-present melting of meta-igneous rocks and the generation of leucogranites – Constraints from garnet major- and trace element data, Lu-Hf whole rock-garnet ages and whole rock Nd-Sr-Hf-O isotope data. *Lithos*, 111, 220–235.

- Kasemann, S., Erzinger, J., & Franz, G. (2000). Boron recycling in the continental crust of the central Andes from the Palaeozoic to Mesozoic, NW Argentina. *Contributions to Mineralogy and Petrology*, *140*, 328–343.
- Kerrick, D. M., & Speer, J. A. (1988). The role of minor element solid solution on the andalusite-sillimanite equilibrium in metapelites and peraluminous granitoids. *American Journal of Science*, *288*, 152–192.
- Kisters, A. F. M., Ward, R. A., Anthonissen, C. J., & Vietze, M. E. (2009). Melt segregation and far-field melt transfer in the mid-crust. *Journal of the Geological Society*, *166*, 905–918.
- Larovere, M. A., delos Hoyos, C. R., Toselli, A. J., Rossi, J. N., Basei, M. A. S., & Belmar, M. E. (2011). High T/P evolution and metamorphic ages of the migmatitic basement of northern Sierras Pampeanas, Argentina: Characterization of a mid-crustal segment of the Famatinian belt. *Journal of South American Earth Sciences*, *31*, 279–297.
- Lork, A., & Bahlburg, H. (1993). Precise U-Pb ages of monazites from the Faja Eruptiva de la Puna Oriental, and the Cordillera Oriental, NW Argentina. In V. A. Ramos (Ed.), *Geología Y Recursos Naturales de Mendoza: 12 Congreso Geológico Argentino Y 2 Congreso de Exploración de Hidrocarburos, Mendoza, Actas 4* (pp. 1–6). Buenos Aires: La Comisión.
- Lucassen, F., & Becchio, R. (2003). Timing of high-grade metamorphism: Early Palaeozoic U-Pb formation ages of titanite indicate long-standing high-T conditions at the western margin of Gondwana (Argentina, 26–29°S). *Journal of Metamorphic Geology*, *21*, 649–662.
- Lucassen, F., Becchio, R., & Franz, G. (2011). The early Palaeozoic high-grade metamorphism at the active continental margin of West Gondwana in the Andes (NW Argentina/N Chile). *International Journal of Earth Sciences*, *100*, 445–463.
- Lucassen, F., Becchio, R., Wilke, H. G., Franz, G., Thirlwall, M. F., Viramonte, J., & Wemmer, K. (2000). Proterozoic-Paleozoic development of the basement of the Central Andes (18–26°S) – A mobile belt of the South American craton. *Journal of South American Earth Sciences*, *13*, 697–715.
- Mahar, E. M., Baker, J. M., Powell, R., Holland, T. J. B., & Howell, N. (1997). The effect of Mn on mineral stability in metapelites. *Journal of Metamorphic Geology*, *15*, 223–238.
- Marchildon, N., & Brown, M. (2003). Spatial distribution of melt-bearing structures in anatexic rocks from Southern Brittany, France: Implications for melt transfer at grain- to orogen-scale. *Tectonophysics*, *364*, 215–235.
- McLellan, E. L. (1988). Migmatite structures in the Central Gneiss Complex, Boca de Quadra, Alaska. *Journal of Metamorphic Geology*, *6*, 517–542.
- Morfin, S., Sawyer, E. W., & Bandyayera, D. (2014). The geochemical signature of a felsic injection complex in the continental crust: Opinaca Subprovince, Quebec. *Lithos*, *196–197*, 339–355.
- O'Connor, J. T. (1965). A classification for quartz-rich igneous rocks based on feldspar ratios. *US Geological Survey Professional Paper USGS*, *B525*, 79–84.
- Otamendi, J. E., & Patiño Douce, A. E. (2001). Partial melting of aluminous metagreywackes in the Northern Sierra de Comechingones, Central Argentina. *Journal of Petrology*, *42*, 1751–1772.
- Otamendi, J. E., Tibaldi, A. M., Vujovich, G. I., & Viñao, G. A. (2008). Metamorphic evolution of migmatites from the deep Famatinian arc crust exposed in Sierras Valle Fértil–La Huerta, San Juan, Argentina. *Journal of South American Earth Sciences*, *25*, 313–335.
- Pankhurst, R. J., Rapela, C. W., & Fanning, C. M. (2000). Age and origin of coeval TTG, I- and S-type granites in the Famatinian belt of NW Argentina. *Transactions of the Royal Society of Edinburgh, Earth Sciences*, *91*, 151–168.
- Patiño Douce, A. E. (1996). Effects of pressure and H₂O content on the compositions of primary crustal melts. *Transactions of the Royal Society of Edinburgh, Earth Sciences*, *87*, 11–21.
- Patiño Douce, A. E., & Harris, N. (1998). Experimental constraints on Himalayan Anatexis. *Journal of Petrology*, *39*, 689–710.
- Pattison, D. R. M. (1992). Stability of andalusite and sillimanite and the Al₂O₃ triple point: Constraints from the Ballachulish Aureole, Scotland. *Journal of Geology*, *100*, 423–446.
- Pattison, D. R. M., & Harte, B. (1988). Evolution of structurally contrasting anatexic migmatites in the 3-kbar Ballachulish aureole, Scotland. *Journal of Metamorphic Geology*, *6*, 475–494.
- Pattison, D. R. M., & Tinkham, D. K. (2009). Interplay between equilibrium and kinetics in prograde metamorphism of pelites: An example from the Nelson aureole, British Columbia. *Journal of Metamorphic Geology*, *27*, 249–279.
- Pearce, M. A., White, A. J. R., & Gazley, M. F. (2015). TCInvestigator: Automated calculation of mineral mode and composition contours for thermocalc pseudosections. *Journal of Metamorphic Geology*, *33*, 413–425.
- Powell, R., & Holland, T. J. B. (1988). An internally consistent dataset with uncertainties and correlations: 3. Applications to geobarometry, worked examples and a computer program. *Journal of Metamorphic Geology*, *6*, 173–204.
- Ramos, V. A. (2008). The basement of the Central Andes: The Arequipa and related Terranes. *Annual Review of Earth and Planetary Sciences*, *36*, 289–324.
- Rapela, C. W., Toselli, A., Heaman, L., & Saavedra, J. (1990). Granite plutonism of the Sierras Pampeanas: An inner cordilleran Paleozoic arc in the southern Andes. In S. M. Kay & C. W. Rapela (Eds.), *Plutonism from Antarctica to Alaska. Geological Society of America Special Paper*, *241*, 77–90.
- Redler, C., White, R. W., & Johnson, T. E. (2013). Migmatites in the Ivrea Zone (NW Italy): Constraints on partial melting and melt loss in metasedimentary rocks from Val Strona di Omegna. *Lithos*, *175–176*, 40–53.
- Reed, S. J. B. (2005). *Electron Microprobe Analysis and Scanning Electron Microscopy in Geology* (2nd ed.). Cambridge University Press.
- Rosenberg, C. L., & Handy, M. R. (2005). Experimental deformation of partially melted granite revisited: Implications for the continental crust. *Journal of Metamorphic Geology*, *23*, 19–28.
- Rossi, J. N., Toselli, A. J., & Durand, F. R. (1992). Metamorfismo de baja presión, su relación con el desarrollo de la cuenca Puncovicana, plutonismo y régimen tectónico, Argentina. *Estudios Geológicos*, *48*, 279–287.
- Rubatto, D., Hermann, J., Berger, A., & Engi, M. (2009). Protracted fluid-induced melting during Barrovian metamorphism in the Central Alps. *Contributions to Mineralogy and Petrology*, *158*, 703–722.
- Sawyer, E. W. (1991). Disequilibrium melting and the rate of melt-residuum separation during migmatization of mafic rocks from the Greenville Front Quebec. *Journal of Petrology*, *32*, 701–738.
- Sawyer, E. W. (1994). Melt segregation in the continental crust. *Geology*, *22*, 1019–1022.

- Sawyer, E. W. (2008). *Atlas of Migmatites: The Canadian Mineralogist. Special Publication 9*. Ottawa, ON, Canada: NRC Research Press, 371 pp.
- Sawyer, E. W. (2010). Migmatites formed by water-fluxed partial melting of a leucogranodiorite protolith: Microstructures in the residual rocks and source of the fluid. *Lithos*, *116*, 273–286.
- Sawyer, E. W., Cesare, B., & Brown, M. (2011). When the continental crust melts. *Elements*, *7*, 229–234.
- Sola, A., & Becchio, R. (2012). Distribución de elementos traza y grado de fusión parcial en migmatitas de la Sierra de Molinos, Salta. *Revista de la Asociación Geológica Argentina*, *69*, 240–251.
- Sola, A. M., Becchio, R. A., & Pimentel, M. M. (2013). Petrogenesis of migmatites and leucogranites from Sierra de Molinos, Salta, Northwest Argentina: A petrologic and geochemical study. *Lithos*, *177*, 470–491.
- Solar, G. S., & Brown, M. (2001). Petrogenesis of migmatites in Maine, USA: Possible source of peraluminous leucogranite in Plutons? *Journal of Petrology*, *42*, 789–823.
- Spear, F. S., Kohn, M. J., & Cheney, J. T. (1999). P-T paths from anatectic pelites. *Contributions to Mineralogy and Petrology*, *134*, 17–32.
- Spear, F. S., Thomas, J. B., & Hallett, B. W. (2014). Overstepping the garnet isograd: A comparison of QuiG barometry and thermodynamic modeling. *Contributions to Mineralogy and Petrology*, *168*, 1–15.
- Spicer, E. M., Stevens, G., & Buick, I. S. (2004). The low-pressure partial-melting behaviour of natural boron-bearing metapelites from the Mt. Stafford area, central Australia. *Contributions to Mineralogy and Petrology*, *148*, 160–179.
- Stevens, G., & Clemens, J. D. (1993). Fluid-absent melting and the roles of fluids in the lithosphere: A slanted summary? *Chemical Geology*, *108*, 1–17.
- Symmes, G. H., & Ferry, J. M. (1995). Metamorphism, fluid flow and partial melting in pelitic rocks from the Onawa Contact Aureole, Central Maine, USA. *Journal of Petrology*, *36*, 587–612.
- Tinkham, D. K., Zuluaga, C. A., & Stowell, H. H. (2001). Metapelite phase equilibria modeling in MnNCKFMASH: The effect of variable Al_2O_3 and $\text{MgO}/(\text{MgO}+\text{FeO})$ on mineral stability. *Geological Materials Research*, *3*, 1–42.
- Vanderhaeghe, O. (2009). Migmatites, granites and orogeny: Flow modes of partially-molten rocks and magmas associated with melt/solid segregation in orogenic belts. *Tectonophysics*, *477*, 119–134.
- Vanderhaeghe, O., & Teyssier, C. (2001). Partial melting and flow of orogens. *Tectonophysics*, *342*, 451–472.
- Vernon, R. H., White, R. W., & Clarke, G. L. (2008). False metamorphic events inferred from misinterpretation of microstructural evidence and P-T data. *Journal of Metamorphic Geology*, *26*, 437–449.
- Vielzeuf, D., Clemens, J. D., Pin, C., & Moinet, E. (1990). Granites, granulites, and crustal differentiation. In D. Vielzeuf & P. Vidal (Eds.), *Granulites and Crustal Evolution*, (pp. 59–85).
- Ward, R., Stevens, G., & Kisters, A. (2008). Fluid and deformation induced partial melting and melt volumes in low-temperature granulite-facies metasediments, Damara Belt, Namibia. *Lithos*, *105*, 253–271.
- Wegmann, M. I., Riller, U., Hongn, F. D., Glodny, J., & Oncken, O. (2008). Age and kinematics of ductile deformation in the Cerro Durazno area, NW Argentina: Significance for orogenic processes operating at the western margin of Gondwana during Ordovician – Silurian times. *Journal of South American Earth Sciences*, *26*, 78–90.
- Wei, C. J., Powell, R., & Clarke, G. L. (2004). Calculated phase equilibria for low- and medium-pressure metapelites in the KFMASH and KMnFMASH systems. *Journal of Metamorphic Geology*, *22*, 495–508.
- Weinberg, R. F., & Hasalová, P. (2015a). Reply to comment by J.D. Clemens and G. Stevens on “Water-fluxed melting of the continental crust: A review”. *Lithos*, *234–235*, 102–103.
- Weinberg, R. F., & Hasalová, P. (2015b). Water-fluxed melting of the continental crust: A review. *Lithos*, *212–215*, 158–188.
- Weinberg, R. F., Hasalová, P., Ward, L., & Fanning, C. M. (2013). Interaction between deformation and magma extraction in migmatites: Examples from Kangaroo Island, South Australia. *Bulletin of the Geological Society of America*, *125*, 1282–1300.
- White, A. J. R., Chappell, B. W., & Cleary, J. R. (1974). Geologic setting and emplacement of some Australian Paleozoic batholiths and implications for intrusive mechanisms. *Pacific Geology*, *8*, 159–171.
- White, R. W., Pomroy, N. E., & Powell, R. (2005). An in situ metatexite-diatexite transition in upper amphibolite facies rocks from Broken Hill, Australia. *Journal of Metamorphic Geology*, *23*, 579–602.
- White, R. W., & Powell, R. (2002). Melt loss and the preservation of granulite facies mineral assemblages. *Journal of Metamorphic Geology*, *20*, 621–632.
- White, R. W., Powell, R., & Clarke, G. L. (2002). The interpretation of reaction textures in Fe-rich metapelite granulites of the Musgrave Block, central Australia: Constraints from mineral equilibria calculations in the system $\text{K}_2\text{O}-\text{FeO}-\text{MgO}-\text{Al}_2\text{O}_3-\text{SiO}_2-\text{H}_2\text{O}-\text{TiO}_2-\text{Fe}_2\text{O}_3$. *Journal of Metamorphic Geology*, *20*, 41–55.
- White, R. W., Powell, R., & Halpin, J. A. (2004). Spatially-focussed melt formation in aluminous metapelites from Broken Hill, Australia. *Journal of Metamorphic Geology*, *22*, 825–845.
- White, R. W., Powell, R., & Holland, T. J. B. (2001). Calculation of partial melting equilibria in the system $\text{Na}_2\text{O}-\text{CaO}-\text{K}_2\text{O}-\text{FeO}-\text{MgO}-\text{Al}_2\text{O}_3-\text{SiO}_2-\text{H}_2\text{O}$ (NCKFMASH). *Journal of Metamorphic Geology*, *19*, 139–153.
- White, R. W., Powell, R., & Holland, T. J. B. (2007). Progress relating to calculation of partial melting equilibria for metapelites. *Journal of Metamorphic Geology*, *25*, 511–527.
- White, R. W., Powell, R., Holland, T., & Worley, J. B. (2000). The effect of TiO_2 and Fe_2O_3 on metapelite assemblages at greenschist and amphibolite facies conditions: Mineral equilibria calculations in the system $\text{K}_2\text{O}-\text{FeO}-\text{MgO}-\text{Al}_2\text{O}_3-\text{SiO}_2-\text{H}_2\text{O}-\text{TiO}_2-\text{Fe}_2\text{O}_3$. *Journal of Metamorphic Geology*, *18*, 497–511.
- White, R. W., Stevens, G., & Johnson, T. E. (2011). Is the crucible reproducible? Reconciling melting experiments with thermodynamic calculations. *Elements*, *7*, 241–246.
- Yardley, B. W. D., & Barber, J. P. (1991). Melting reactions in the Connemara Schists: The role of water infiltration in the formation of amphibolite facies migmatites. *American Mineralogist*, *76*, 848–856.

SUPPORTING INFORMATION

Additional Supporting Information may be found online in the supporting information tab for this article.

Figure S1. Ti-in-biotite thermometry (Henry et al., 2005) for metapelites samples from different metamorphic

zones from Sierra de Molinos (see text for details). Estimated temperature increases with metamorphic zones from (a) through to (c). Samples numbers are given in boxes in each figure. In (c) biotite is divided into inclusions and matrix.

Figure S2. Ternary diagrams comparing chemical composition of sample MO40_10408 metapelite from Sierra de Molinos with Puncoviscana Formation from several localities (Do Campo & Guevara, 2005; 16 metapelite samples) on a molar proportion basis. Average value for X_{Al} [$Al_2O_3/(Al_2O_3+FeO+MgO)$] and X_{Ca} [$CaO/(CaO+K_2O+Na_2O)$] for Puncoviscana Formation is 0.53 and 0.12, respectively, and similar to our reference metapelite with $X_{Al} = 0.52$ and $X_{Ca} = 0.16$.

Table S1. The complete electron microprobe mineral chemistry dataset.

Table S2. Melt compositions calculated for dehydration melting and H_2O -fluxed melting at conditions shown in Figure 12d.

How to cite this article: Sola AM, Hasalová P, Weinberg RF, et al. Low- P melting of metapelitic rocks and the role of H_2O : Insights from phase equilibria modelling. *J Metamorph Geol.* 2017;00: 1–29. <https://doi.org/10.1111/jmg.12279>